NATIONAL ADVISORY COMMITTEE FOR AERONAUTICS

WARTIME REPORT

ORIGINALLY ISSUED

February 1942 as
Advance Restricted Report

WIND-TUNNEL INVESTIGATION OF CARBURETOR-AIR INLETS

By W. J. Nelson and K. R. Czarnecki

Langley Memorial Aeronautical Laboratory
Langley Field, Va.

WASHINGTON

WIND-TUNNEL INVESTIGATION OF CARBURETOR-AIR INLETS

By W. J. Nelson and K. R. Czarnecki

INTRODUCTION

An investigation of the internal and external airflow characteristics of carburetor-air inlets for liquid-cooled engine installations has been conducted in the NACA full-scale wind tunnel. Increased airplane speeds and higher operational altitudes have augmented the difficulties in the design of air inlets that are efficient over the entire flight range. Efficient inlets provide a uniform velocity distribution at the carburetor metering venturi with high ramming pressure and a low external drag.

Full-scale models of two representative pursuit airplanes were used in the investigation of nine carburetor-air inlets differing in shape, size, and location. The inlet positions were confined to the forward section of the fuselage. The effects of propeller operation on the inlet characteristics were determined for most of the installations. Measurements of velocity distribution, ram, and drag were made at air quantities and angles of attack corresponding to a wide range of flight conditions for each of these inlets.

APPARATUS AND TESTS

A description of the NACA full-scale wind tunnel and balance used for these tests is given in reference 1. The models were mounted in the test section as shown in figure 1. The principal dimensions of the models are given in figures 2 and 3. A 10-foot-diameter propeller, fitted with cuffs (fig. 4), and driven by an electric motor, was used on model A to determine the effect of the slipstream.

The duct system ahead of the nominal carburetor location was made in two sections; one section formed the inlet and the diffuser and the other contained the bend and the connection with the carburetor flange. Changes in the installation during the tests were confined to the inlet and the diffuser. (See figs. 5 to 15.) All the scoops were of conventional design except scoop 5, which twisted so that the inlet was alined with the direction of the slipstream in the high-speed condition.

Since no engine was provided in these models, it was necessary to add a duct replacing the carburetor to provide an adjustable outlet with which to control the air flow through the installation. The duct installation in model A is shown by an isometric drawing in figure 16; in figures 17 and 18 the details of the bends ahead of the carburetor are given for both models.

The increment of drag added by each duct installation was determined from the difference between force measurements on the bare model and on the model with the carburetor-air system installed. These tests were made over a range of lift coefficients from -0.2 to 0.5 at tunnel speeds of 63 and 100 miles per hour.

The velocity distribution and the ramming pressure at the carburetor were obtained from measurements of total and static pressure at the flange location shown in figure 16. A grid of 29 total- and static-pressure tubes of 1/16-inch diameter was placed in the outlet to provide data for the calculations of internal drag and air quantity. The static-pressure measurements required for the determination of the critical Mach number on the upper lip (table I) of each of the inlets and at the scoop-fuselage fillets of scoop 5 were obtained by means of 1/32-inch-diameter orifices installed flush with the surfaces.

Power-on tests were made under conditions simulating high-speed and climbing flight to determine the effect of the slipstream on the available ramming pressure, the inlet velocity, and the surface pressures. At the high-speed lift coefficient of 0.1, estimated for the airplane equipped with a 1600-horsepower engine, the propeller blade angle and V/nD were calculated to be 60° and 2.96, respectively. In the climb condition, for a lift coefficient of 0.5, the calculated blade angle and V/nD were 40° and 1.32. The test airspeeds corresponding to the high-speed and climb conditions were 63 and 45 miles per hour, respectively.

SYMBOLS

ΔC_D increment of drag coefficient due to scoop

C_{D_e} calculated increment of drag coefficient due to external drag

C_{D_i} calculated increment of drag coefficient due to internal drag

C_L lift coefficient

S wing area

H_c total pressure at carburetor position

H_o free-stream total pressure

p surface pressure

q local dynamic pressure

q_o free-stream dynanic pressure

V_i inlet velocity

V_o free-stream velocity

Q air quantity

M_c critical Mach number

α angle of attack

β propeller blade setting at 0.75 radius

D propeller diameter

n speed of propeller rotation

T propeller thrust

T_c thrust coefficient $(T/\rho V_o^2 D^2)$

RESULTS AND DISCUSSION

A typical set of tuft observations made at the entrance of scoop 3 and presented in figure 19 illustrates the importance of the inlet-velocity ratio V_i/V_o as a fundamental parameter in the inlet design. The tuft observations at the low value of $V_i/V_o = 0.21$ show that the boundary layer at the center of the scoop separates from the fuselage, resulting in the formation of a thick layer of eddying flow at the bottom of the inlet which upsets the main flow into the duct. Boundary-layer separation at the inlet

occurs when the inlet static pressure $q_o [1 - (V_i/V_o)^2]$ exceeds the total pressure of the fluid in the boundary layer approaching the inlet. The pressure at the inlet varies from stagnation pressure at an inlet-velocity ratio of zero to stream static pressure at an inlet-velocity ratio of 1.00. The dependency of boundary-layer separation on the inlet-velocity ratio is shown in figures 19(b) and 19(c) in which, for $V_i/V_o = 0.36$, the pressure rise at the inlet was insufficient to cause large-scale separation and, for $V_i/V_o = 0.53$, the boundary layer entered the scoop with no indication of unstable flow.

Although the inlet-velocity ratio is one of the most fundamental inlet parameters, direct comparison of the various scoops cannot be made on this basis alone. At a given V_i/V_o a larger air quantity enters the larger inlets and, consequently, the duct losses, which are primarily a function of internal dynamic pressure, are higher. The parameter Q/V_o, in which Q is the air-flow volume, provides a basis for comparison of the duct installations as a function of the air-flow quantity.

Air Flow and Ram

Contours of total pressure (figs. 20 to 26) at the flange location are given for all the installations tested to facilitate the visualization of the air flow at the carburetor. The average value of the total pressure at the carburetor is the ramming pressure, which is given as a percentage of the free-stream dynamic pressure. Since the static pressure was uniform in most of the tests, the contours also approximately indicate the velocity distribution at the metering venturi. The ram obtained with the better scoops on airplane A was consistently lower than that obtained with similar scoops on airplane B, as a result of the higher bend losses that occurred at the abrupt duct bend on airplane A, as compared with those caused by the larger radius bend on airplane B (figs. 17 and 18).

The total-pressure distribution, which was essentially uniform for all the protruding scoops at low inlet-velocity ratios, became increasingly irregular at higher values of V_i/V_o. The uniformity of flow at very low-flow ratios is due to mixing in the diffuser as a result

of a turbulent condition at the inlet and to the low losses at the duct bend. At inlet-velocity ratios below about 0.30, the desirable flow uniformity is accompanied by an undesirable loss of ram owing to the flow breakdown at the duct inlet. For larger values of the inlet-velocity ratio from approximately 0.30 to 0.50, optimum over-all performance of the scoop is attained with a uniform velocity distribution at the carburetor and maximum ramming pressure.

As the flow through the carburetor system is increased with greater values of V_i/V_o and Q/V_o, the duct bend losses become larger, tending to decrease both the flow uniformity and the available ram. At the bend the greater part of the energy losses occur on the inner side of the turn because of separation of flow around the small inner radius. This effect is shown for scoop 1 (fig. 20) at a V_i/V_o value of 1.13 and a Q/V_o value of 0.16. The pressure available behind the inside of the turn was about 20 percent less than at the outside of the turn, and the average ram was 78.5 percent q_o as compared with 91.5 percent q_o for a flow ratio of 0.05. The same effects are clearly shown in figures 21 to 24.

An analysis of the source of the loss of ram is made in figure 27, in which the pressure in the carburetor has been plotted against V_i/V_o for inlets 1, 3, 4, and 5. Because of difference in inlet area, the flow quantities at the same inlet-velocity ratios for the several scoops are different.

These data all show the characteristic decrease in ram with increasing inlet-velocity ratio with the effect accentuated for the large-area inlet scoops. In the analysis of the data it was assumed that the losses in the bend were proportional to the local dynamic pressure and, based on studies of bends, it was estimated that the loss in the case of the abrupt bend in model A would be 40 percent q.

The bend losses, calculated on the foregoing assumption, are shown in figure 27. It will be noted that, for the high-flow quantity, the bend loss accounts for a large part of the total loss in ram with a smaller, more nearly constant amount caused by the boundary-layer and duct losses. At very low inlet-velocity ratios the bend losses are small and, as previously mentioned, the low ram is due to separation at the inlet. The extent of the dissymmetry occurring at the carburetor for the high flow ratios will largely de-

pend on the efficiency of the bend. The results indicate that in high-altitude flight, for which case the duct velocities may become high, extreme care must be exercised in the design of the duct to avoid large losses in ram and loss in flow uniformity.

The data obtained on scoops 6, 7, and 8, tested on model B, are of particular interest in demonstrating the effect of the inlet position with reference to the fuselage surface. Scoop 6 was so located that the inlet area was entirely above the surface with a narrow gutter provided for bypassing the boundary layer; scoop 7 was so mounted that the local surface of the inlet was tangent to the surface of the fuselage; and inlet 8 was flush with the upper contour of the fuselage with no protruding scoop. The rams obtained with scoops 6 and 7 were both high and about the same (fig. 25). For the flush inlet 8, only 73.5 percent q_o was recovered as ram and the velocity distribution at the carburetor was very irregular. The pressure at the inside of the turn was only about half the stream pressure, indicating a breakaway flow ahead of the duct inlet. In effect the external stream overruns the inlet, that is, it fails to make an efficient turn without the guiding action of the protruding scoop. On the basis of ram and velocity distribution, scoops 6 and 7 are of equal merit; as will be noted later, however, the drag of the scoop with the gutter is higher.

The effect of decreasing the height of the duct inlet while maintaining a comparable inlet area is shown in figure 27. At low values of V_i/V_o the flat scoop has about the same effectiveness as the scoops that protruded farther above the surface; at high values of V_i/V_o, however, the ram is largely decreased. This result is attributed to the greater length of fuselage surface from which the boundary layer is taken, resulting in a larger percentage of the air entering the duct at a reduced total pressure. Additional factors contributing to the low rams at high-flow quantities are the less favorable expansions in the duct diffuser and the small hydraulic radius caused by the flat shape with resultant increased skin friction.

The results obtained with the unconventional annular inlet 9 are shown in figure 26. At angles of attack corresponding to the high-speed condition, this inlet has characteristics comparable with the best protruding scoops. At high angles of attack, however, owing to the shielded

position of the inlet above the propeller spinner and to the tendency of the flow to spill out of the top of the cowling, the pressure in the scoop is greatly reduced. It will be noted that, at angle of attack of 12°, the ram has dropped to approximately 30 percent of the stream pressure. In the case of the protruding scoop 5 (fig. 28), a decrease of only about 5 percent in ram occurred over an angle-of-attack range of 11°. Similar results were obtained with other protruding scoops.

The effect of the slipstream on the ramming pressure available at the carburetor is shown for scoops 1 to 5 in figure 29. At a simulated high-speed operating condition, the slipstream increased the carburetor ram approximately 5 percent q_o for the five inlets tested. In the climb condition, a slightly greater increment was measured. The failure to recover a larger percentage of ram pressure in the climb condition may be accounted for by inefficient action of the lower section of the propeller cuff.

The improvement in power-on ram made by twisting the inlet into the slipstream is shown in figure 30. In the high-speed condition at an inlet-velocity ratio of 0.40 an increase of approximately 3 percent q_o was measured.

Drag

A summary of the drag data for the various carburetor-air duct installations is given in table II. The increments ΔC_D in the table are the differences between measured drag coefficients of the model with and without the carburetor-air systems and include the drag due to flow through the outlet duct and the outlet losses. The values of the drag increments given are therefore useful only for comparing different scoop arrangements on the same model; hence the values of ΔC_D for installations on model B cannot be compared with those on model A because of differences in the outlet duct system. The outlet for model A was relatively efficient at low air-flow quantities; at large values of Q/V_o, however, the carburetor air was ejected from the fuselage at a large angle to the stream direction producing a turbulent region behind the outlet with high drag. On model B, the outlet duct was unavoidably tortuous and a large part of the kinetic energy of the air flow was lost, resulting in a high outlet drag.

The evaluation of the internal and external components of the drag has been accomplished by calculating the energy lost in the duct and deducting this quantity from the measured ΔC_D. The internal drag coefficient C_{D_i}, corresponding to the losses in the duct system up to the carburetor flange, is given by the expression

$$C_{D_i} = \frac{2Q}{SV_o}\left[1 - \sqrt{\frac{H_c}{H_o}}\right]$$

In a similar way the drag coefficient corresponding to the total loss between the inlet and the outlet can be calculated by replacing the term H_c in the foregoing equation by the value of the total pressure at the duct outlet. The values of C_{D_i} for the different carburetor installations are given in table II, in which it will be noted that the drag due to loss ahead of the carburetor is small.

The values of the drag coefficients corresponding to the total internal duct losses are not tabulated. They were calculated, however, and the external drag coefficient increment C_{D_o} was obtained by deducting the total internal drag coefficient from the drag coefficient increment measured in the force test. As previously mentioned, the external drag coefficients include the losses occurring at the outlet and are therefore larger than for normal installations with engines. The results indicate, with respect to measurements at low airspeeds, that the drags of the different scoops tested are somewhat similar and that an efficient installation of a carburetor scoop on a conventional pursuit airplane should not increase the drag coefficient by more than 1 percent.

Compressibility

As a result of numerous fundamental aerodynamic investigations, a technique has been evolved in which pressure measurements at low airspeeds are used to estimate the speed at which compressibility effects become critical. This critical speed has been defined as the forward speed at which the local velocity at any point on a body reaches the speed of sound; at speeds below the critical a well-defined variation of pressure distribution with speed occurs that is accompanied by significant drag changes. The drags of the scoops as measured in this investigation

at 100 miles per hour may be increased considerably at higher airplane speeds, if the local speed of sound is approached at any point on the scoop.

The method of estimating the critical speed from measurements of the pressures at low speeds is given in reference 2. The value of the maximum negative pressure is determined by means of surface pressure measurements at low speeds and this value is extrapolated to high Mach numbers as in figure 31. The critical speed is determined by the intersection of the extrapolated pressure curve with the curve of the local speed of sound.

Examination of figure 31 shows that the highest critical speeds will be obtained with scoops having the lowest maximum negative pressures. The problem of designing a scoop with a high critical speed is analogous to that of designing an airfoil with the same characteristics because, as in the case of an airfoil, the pressures are determined by the camber of the lip, its thickness, and its angle of attack. The angle of attack at the scoop inlet is determined by the amount of flow that passes through and around the inlet which is expressed by the ratio V_i/V_o. At low values of V_i/V_o the angle of attack is high and the converse also holds (fig. 32). Minimum negative pressures would be obtained for a thin-lip scoop adjusted throughout the flight range so as always to operate at its ideal angle of attack. In the usual case, however, adjustable inlet scoops are undesirable and the optimum scoop becomes a compromise for best average operation over the flight range, with the specific requirement that a critical speed on the scoop lip must exceed that of the rest of the airplane. The compromise involved in the design of fixed-area inlet scoops requires discarding thin scoop lips because of their known undesirable sensitivity to changes in angle of attack. In the present investigation, sufficient thickness was provided at the scoop lips to minimize the variation in pressure distribution with the inlet-velocity ratio.

The pressure distributions measured on the scoops tested in this investigation for a range of scoop lip shapes and inlet-velocity ratios are shown in figures 33 to 41. In the analysis of the results for the different scoop modifications, the minimum negative pressure peaks occur on the contours that provide the most uniform pressure distribution. This uniform pressure distribution is associated with shapes that are correctly cambered for

the angle of attack at which they are operating. In general, the peak pressures are decreased by increasing the radius of curvature in the region of negative pressure.

The lower peak pressures accompanying the increased values of inlet-velocity ratio are shown in figures 36 to 40. In the case of scoop 1 with the original contour, the peak negative pressure is decreased from 0.97 q_o to -0.41 q_o for a variation in the inlet-velocity ratio from 0.34 to 1.13. This result corresponds to a change in critical Mach number from 0.59 to 0.74, which is equivalent to an increase in the critical speed from 411 to 510 miles per hour at 25,000 feet altitude. A similar variation of critical speed with inlet-velocity ratio occurs for the other scoops. The critical variation of the pressure distribution on the inlet with the inlet-velocity ratio may lead to the use of adjustable scoops for efficient operation over wide ranges of speed and altitude.

The effects of propeller operation on the pressure distribution on twisted scoop 5 are shown in figures 39 and 40. Along the left fillet, the side from which the propeller approaches the scoop, a small decrease in the maximum negative pressure was caused by the slipstream at the simulated high-speed condition (fig. 39). The pressures along the top of the scoop and in the right fillet were not greatly affected. With the increased slipstream velocity simulating the climb condition (fig. 40), a further reduction of the negative pressures in the left fillet occurred accompanied by slight reductions in the peak pressures on the top and on the right fillet. For the tests with the inlet-velocity ratio of about 1.00, the peak negative pressures occurred on the inside lip of the scoop due to the negative angle at which the lip was operating.

CONCLUSIONS

From the results obtained for eight scoops tested in the full-scale tunnel, it has been concluded:

1. The important design parameters that determine the operational characteristics of carburetor-air scoops are the inlet-velocity ratio V_i/V_o and the air-flow quantity Q/V_o.

2. Flow separation occurs in the boundary layer ahead of the carburetor inlet if the inlet-velocity ratio is decreased below about 0.30.

3. Highest over-all inlet efficiencies occur for values of V_i/V_o between 0.40 and 0.50.

4. One of the most important sources of loss of ram and nonuniformity of flow at the carburetor is the duct bend. The velocity at the duct bend should be reduced to as low a magnitude as feasible.

5. Raised carburetor scoops with gutters for bypassing the boundary layer show no important increases in ram over well-designed scoops that are tangent to the fuselage. The drag of the raised scoop is higher.

6. Lower ram and less uniform velocity distribution were obtained with wide flat scoops at high inlet-velocity ratios.

7. The drag of a well-designed carburetor air scoop should not exceed 1 percent of the airplane drag.

8. The minimum negative pressure peaks and highest critical speed are obtained on scoop contours that provide a uniform pressure distribution. Highest critical speeds are reached at high inlet-velocity ratios.

9. The critical variation of the pressure distribution on the inlet with V_i/V_o may lead to the use of adjustable scoops for efficient operation over wide ranges of speed and altitude.

Langley Memorial Aeronautical Laboratory,
National Advisory Committee for Aeronautics,
Langley Field, Va.

REFERENCES

1. DeFrance, Smith J.: The N.A.C.A. Full-Scale Wind Tunnel. Rep. No. 459, NACA, 1933.

2. von Kármán, Th.: Compressibility Effects in Aerodynamics. Jour. Aero. Sci., vol. 8, no. 9, July 1941, pp. 337-356.

TABLE I.

SCOOP LIP

SECTIONS

All dimensions are in inches

Station x	Upper surface, y											
	Scoop 1				Scoop 3			Scoop 4		Scoop 5		
	Orig.	A	B	C	Orig.	A	B	Orig.	A	West	C.L.	East
0	0.72	0.74	0.62	0.64	0.77	0.69	0.59	0.57	0.54	1.00	0.83	1.82
.25	.92	.97	.92	.89	.99	.97	.95	.76	.80	----	1.00	----
.50	1.09	1.15	1.15	1.25	1.15	1.20	1.20	.93	1.00	1.29	1.15	2.22
.75	1.24	1.31	1.34	1.45	1.32	1.39	1.40	1.10	1.17	----	1.27	----
1.00	1.38	1.44	1.48	1.52	1.46	1.54	1.57	1.24	1.31	1.48	1.37	2.56
1.25	1.50	1.58	1.63	1.67	1.58	1.69	1.73	1.37	1.44	----	1.49	----
1.50	1.62	1.70	1.74	1.80	1.70	1.81	1.89	1.52	1.59	1.61	1.59	2.88
1.75	1.72	1.81	1.86	1.92	1.80	1.91	1.99	1.62	1.69	----	1.67	----
2.00	1.84	1.91	1.96	2.00	1.89	2.02	2.10	1.73	1.80	1.69	1.75	3.15
2.50	2.00	2.09	2.15	2.20	2.05	2.17	2.25	1.91	1.98	1.73	1.89	3.43
3.00	2.14	2.23	2.30	2.44	2.17	2.31	2.39	2.04	2.11	1.76	2.00	3.72
3.50	2.27	2.37	2.43	2.49	2.27	2.41	2.49	2.17	2.24	1.78	2.11	3.95
4.00	2.40	2.50	2.55	2.61	2.35	2.50	2.58	2.28	2.35	1.80	2.19	4.22
4.50	2.50				2.42	2.57	2.65	2.38	2.45	1.80	2.26	4.46
5.00	2.58				2.47	2.63	2.71	2.47	2.54	1.77	2.33	4.70
5.50	2.65				2.52	2.67	2.75	2.55	2.62	1.75	2.38	----
6.00	2.74				2.56	2.71	2.79	2.68	2.61	1.73	2.43	5.13
7.00	2.87				2.63	2.79	2.87	2.75	2.82		2.52	
8.00	2.98										2.60	
9.00	3.06										2.66	
R	.45	.40	.32	.22	.45	.32	.23	.38	.30	.68	.57	1.06
x_i [a]		.09	.15	.22		.14	.22		.07			
y_i [a]			.05	.08		.07	.09					
θ, deg.	28	30	28	29	25	24	30	7	8	6	5	0

[a] x_1 and y_1 = ordinates of center of leading-edge radius of modified inlets with respect to center of original lip.

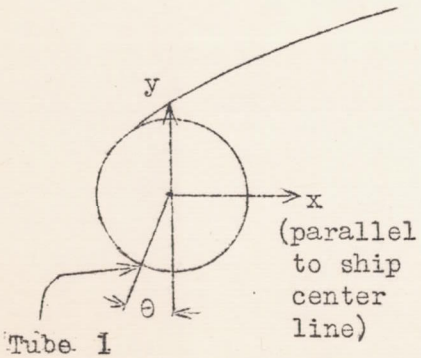

TABLE II

SUMMARY OF DRAG DATA

Scoop	Inlet-area (sq in.)	V_i/V_o	Q/V_o	ΔC_D at $C_L=0.1$ Test speed (mph)		C_{D_i}	C_{D_e} at $C_L=0.1$ Test speed (mph)	
				63	100		63	100
1	19.8	0.49	0.067	0.0004	0.0002	0.00004	0.0004	0.0002
2	30.3	.32	.067	.0001	.0002	.00004	.0001	.0002
3	47.3	.21	.069	.0003	-----	.00007	.0002	-----
		.31	.102	.0004	-----	.00008	.0003	-----
		.33	.108	.0005	.0006	------	.0004	.0005
		.36	.118	.0003	-----	.00008	.0002	-----
		.43	.141	.0003	-----	.00011	.0001	-----
		.50	.164	.0007	-----	.00016	.0004	-----
		.53	.174	.0010	-----	.00019	.0006	-----
4	32.7	.27	.061	-----	.0003	.00005	-----	.0003
5	26.3	.37	.068	.0003	.0003	.00003	.0003	.0003
		.54	.099	.0003	.0003	.00005	.0003	.0002
6	37.1	.26	.067	-----	.0008	.00001	-----	-----
		.34	.088	-----	.0007	.00001	-----	-----
		.45	.116	-----	.0008	.00003	-----	-----
7	26.9	---	----	-----	-----	------	-----	-----
		.37	.068	-----	.0001	.00001	-----	-----
		.55	.103	-----	.0003	.00001	-----	-----
		.66	.123	-----	.0005	.00002	-----	-----
8	27.8	.42	.081	-----	.0002	.00014	-----	-----
		.52	.100	-----	.0005	.00019	-----	-----

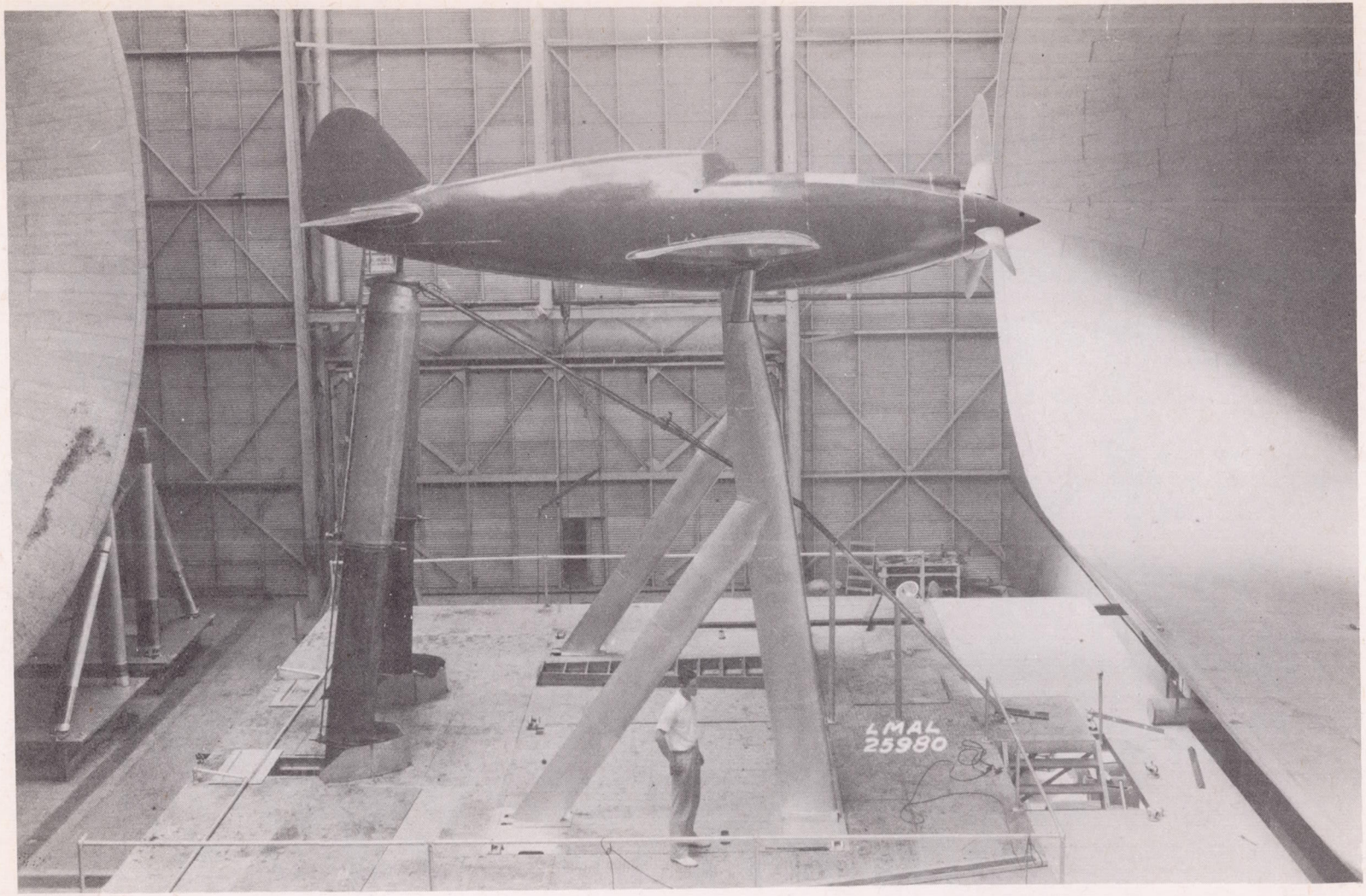

Figure 1.- Model A with carburetor air scoop 1, as tested in the full-scale wind tunnel.

NACA

Fig. 2

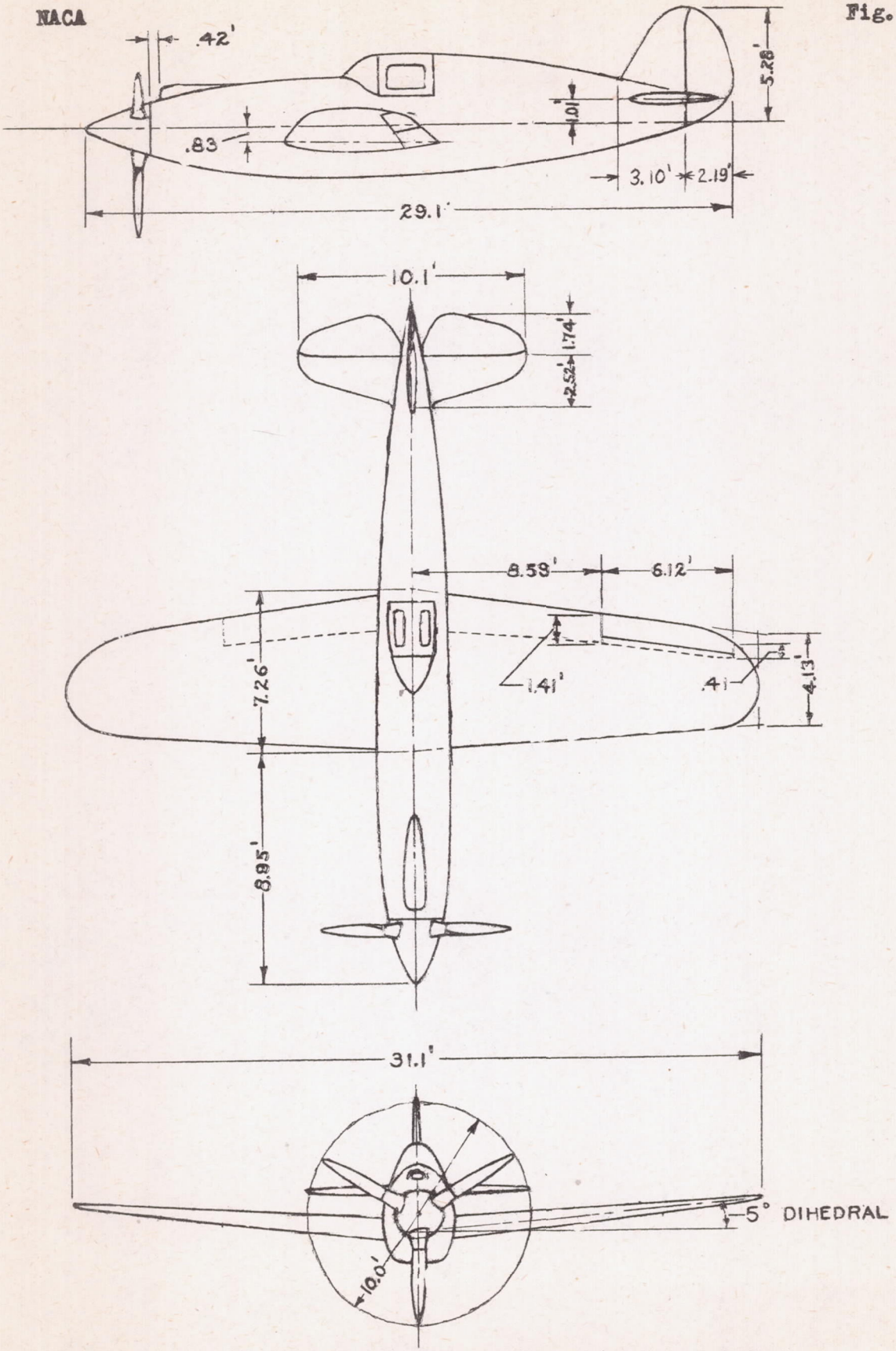

Figure 2.- General arrangement of model A.

NACA

Fig. 3

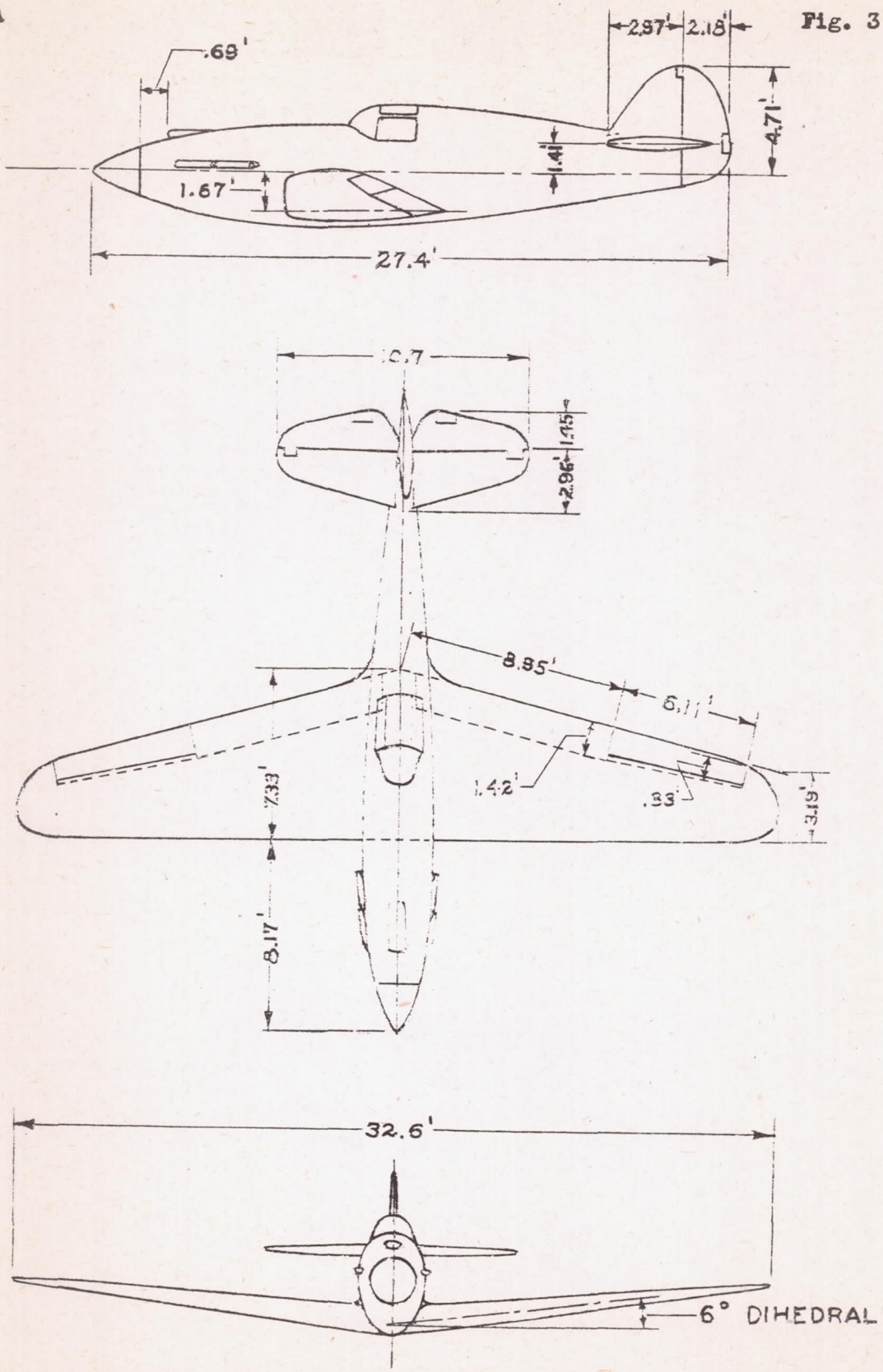

Figure 3.- General arrangement of model B.

NACA

Fig. 4

Section A

x	y_U	y_L
0	0	0
0.116	0.280	0.250
.232	.390	.315
.463	.535	.405
.694	.645	.465
.925	.745	.510
1.487	.890	.565
1.850	.990	.595
2.315	1.065	.600
2.775	1.110	.595
3.700	1.135	.575
4.625	1.095	.540
5.560	1.000	.465
6.475	.840	.385
7.410	.625	.280
8.330	.360	.165
9.250	0	0

$R_{L.E.} = 0.335$

$R_{T.E.} = 0.058$

Section B

x	$y_U = y_L$
0	0
0.194	.430
.388	.625
.775	.930
1.163	1.160
1.550	1.340
2.330	1.635
3.100	1.845
3.880	2.000
4.650	2.110
6.200	2.190
7.750	2.100
9.300	1.840
10.850	1.465
12.400	1.025
13.950	.535
15.500	0

$R_{L.E.} = 0.520$

$R_{T.E.} = 0$

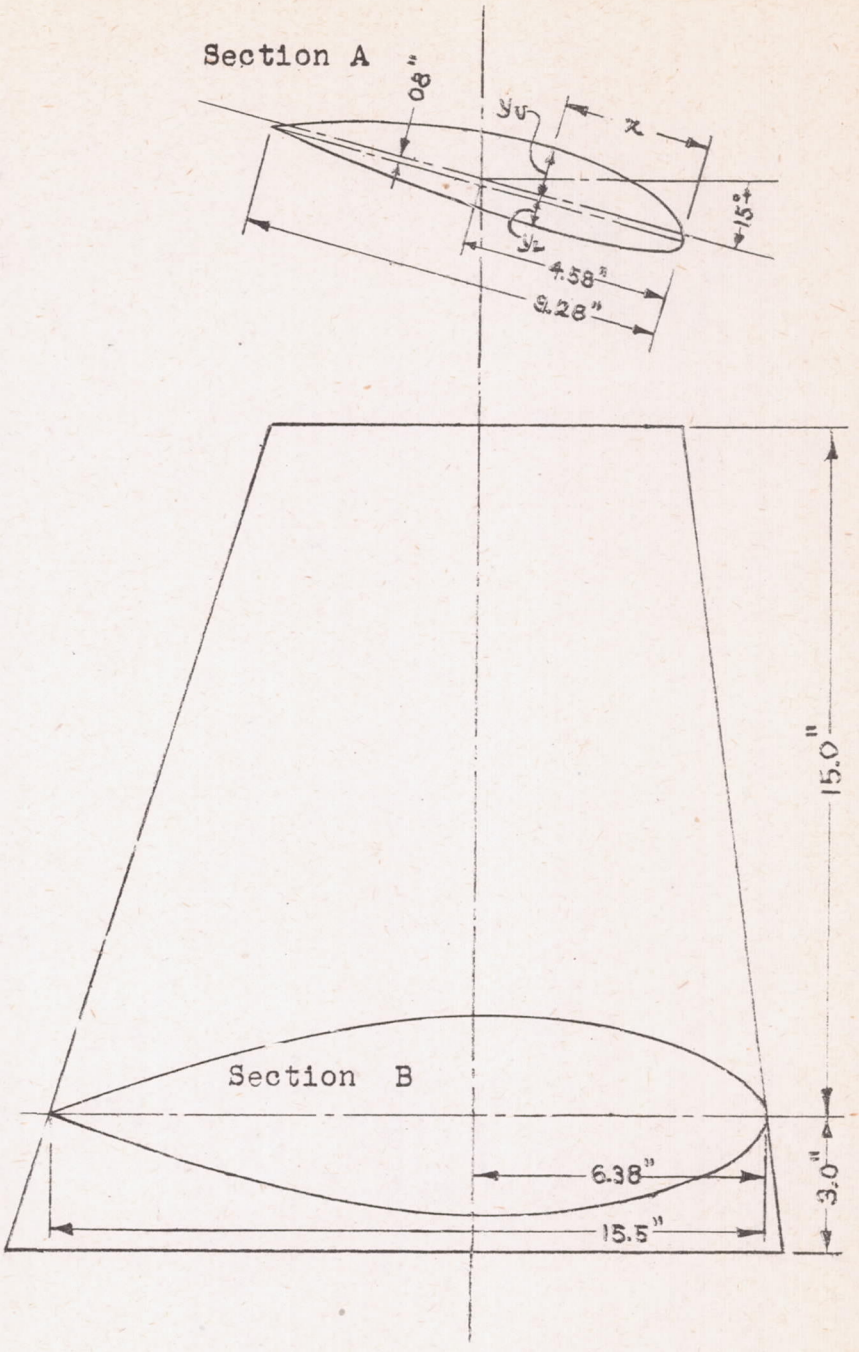

Figure 4.- Dimensions of propeller cuff.

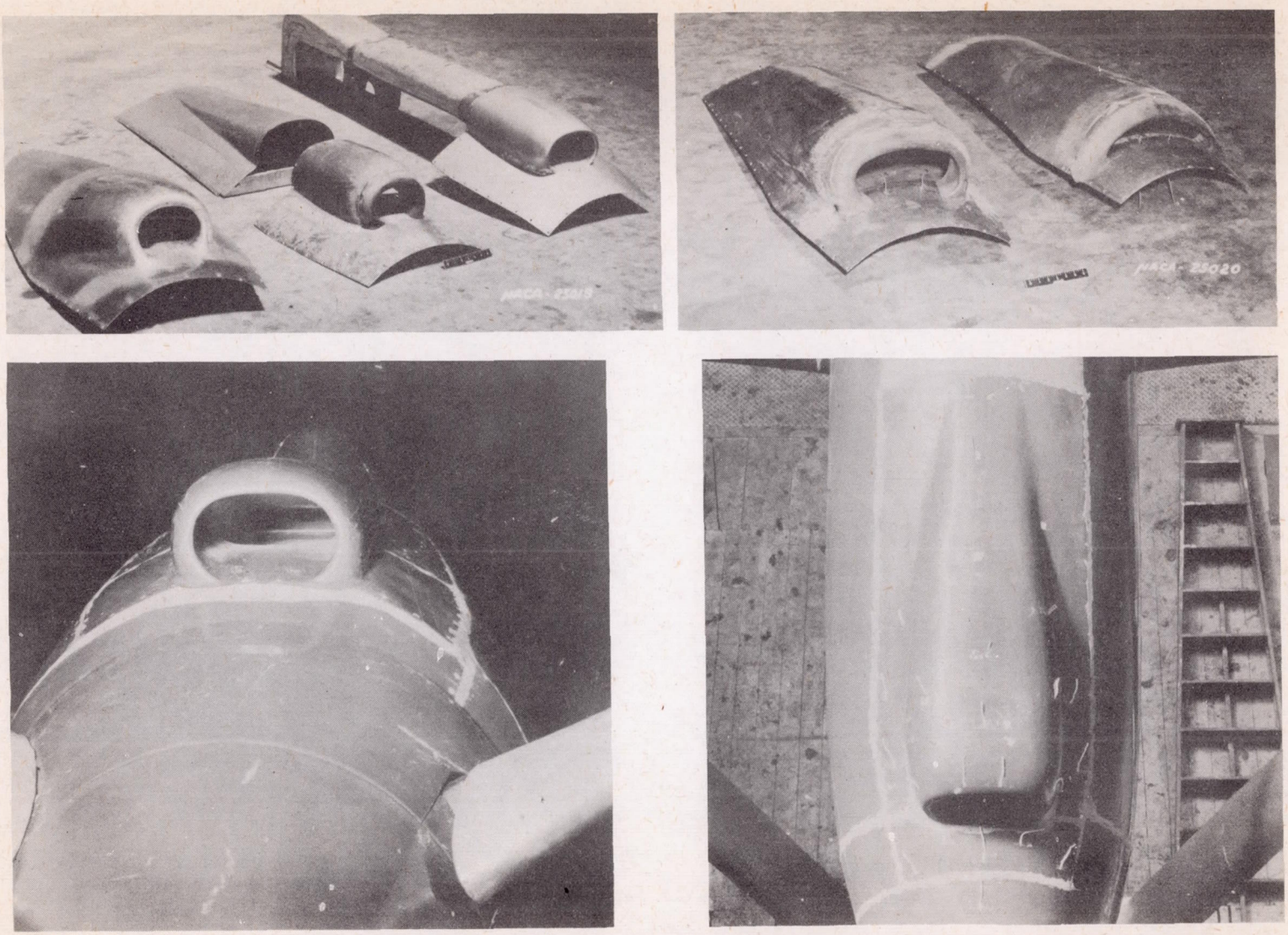

Figure 5.- Carburetor air scoops tested on model A.

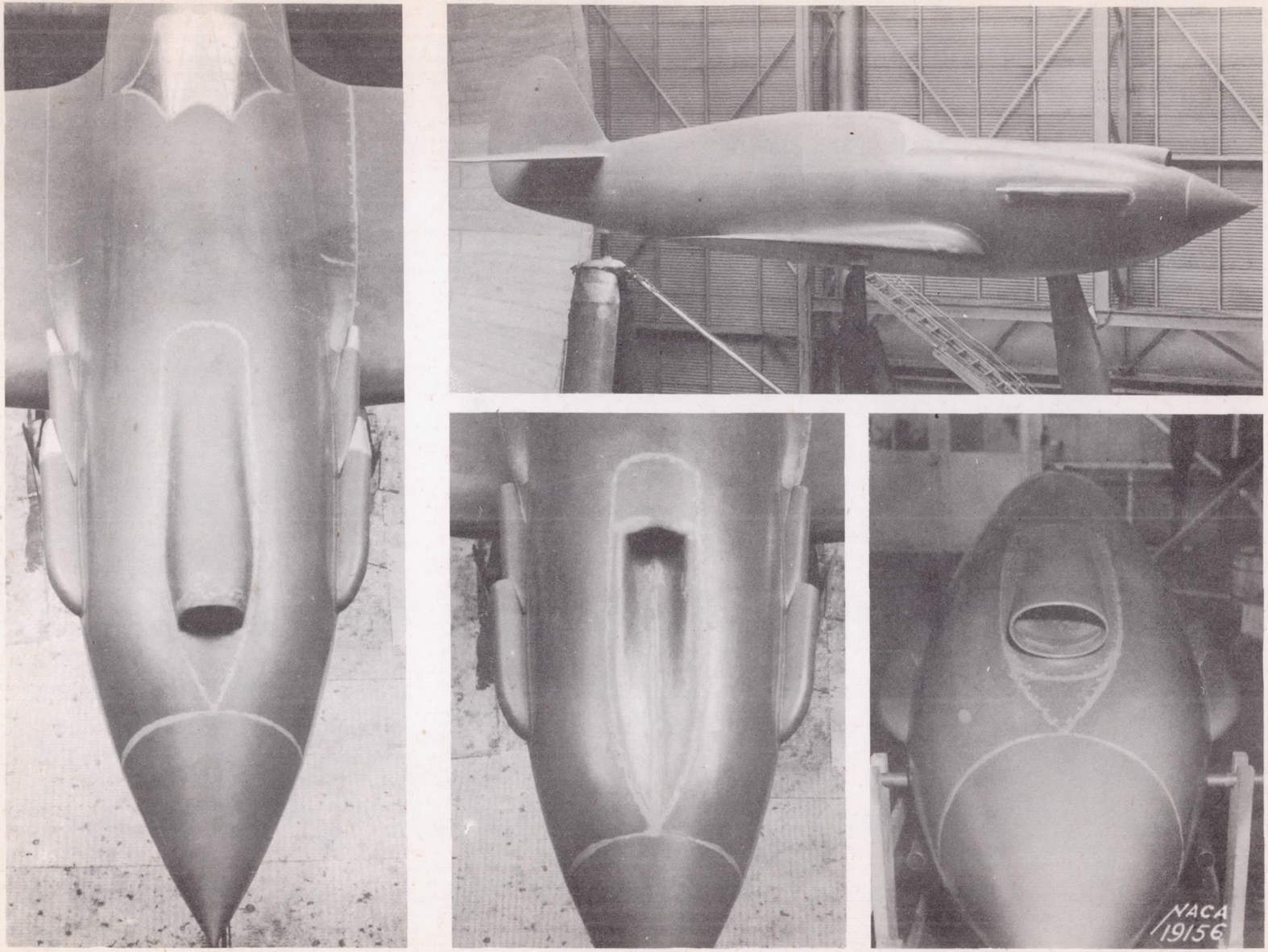

Figure 6.- Model B and scoops 6, 7, and 8.

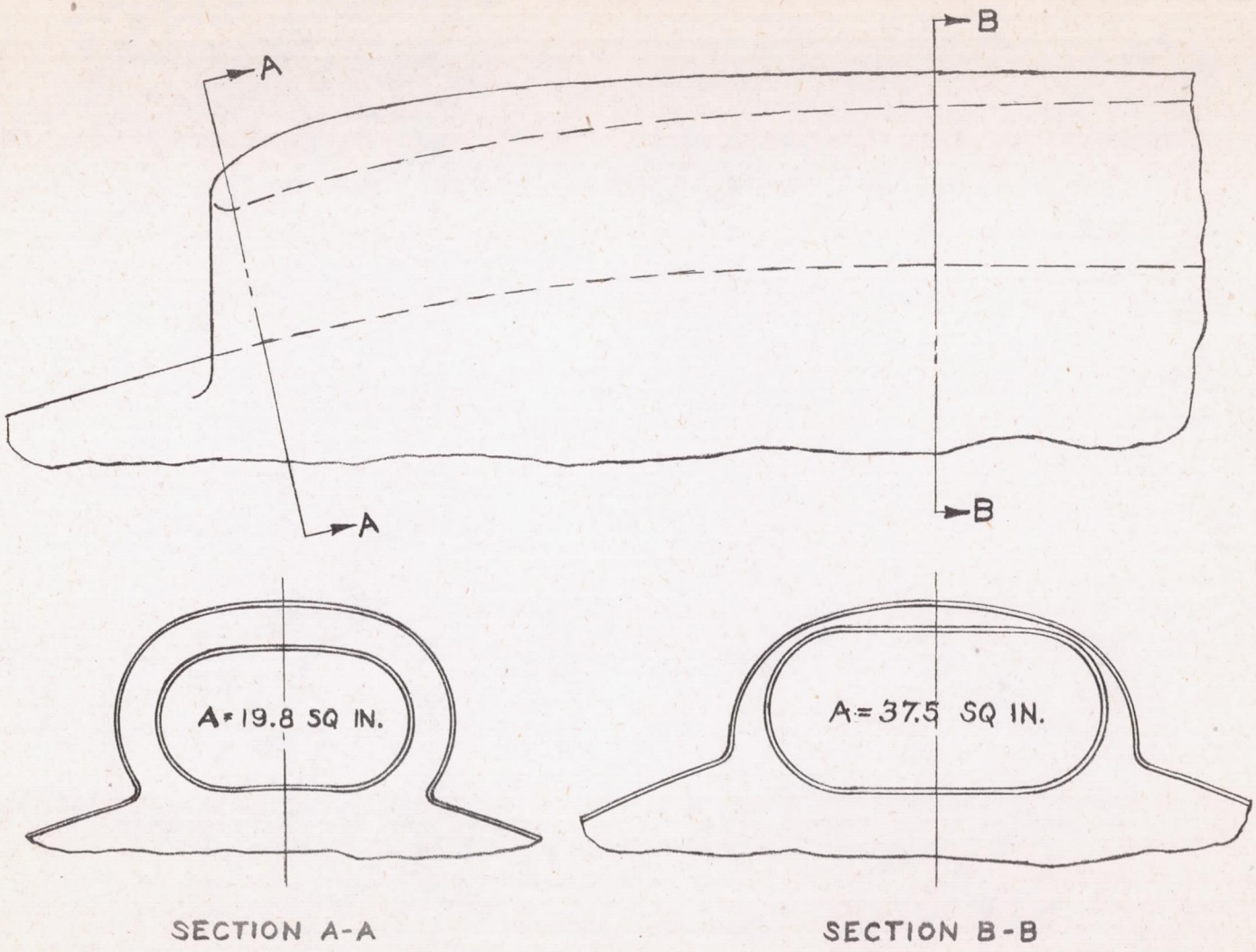

Figure 7.- Carburetor air scoop 1, tested on model A.

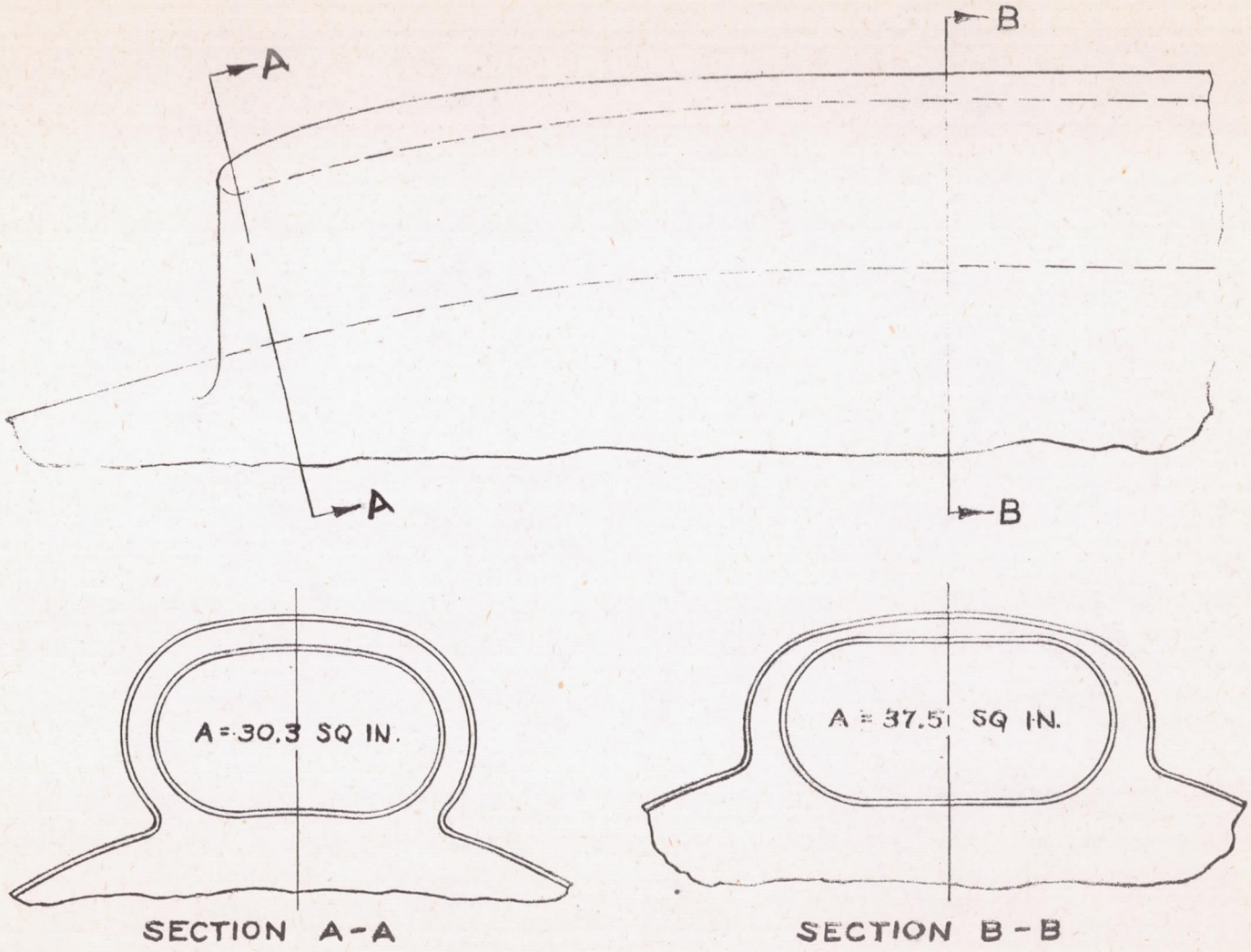

Figure 8.- Carburetor air scoop 2, tested on model A.

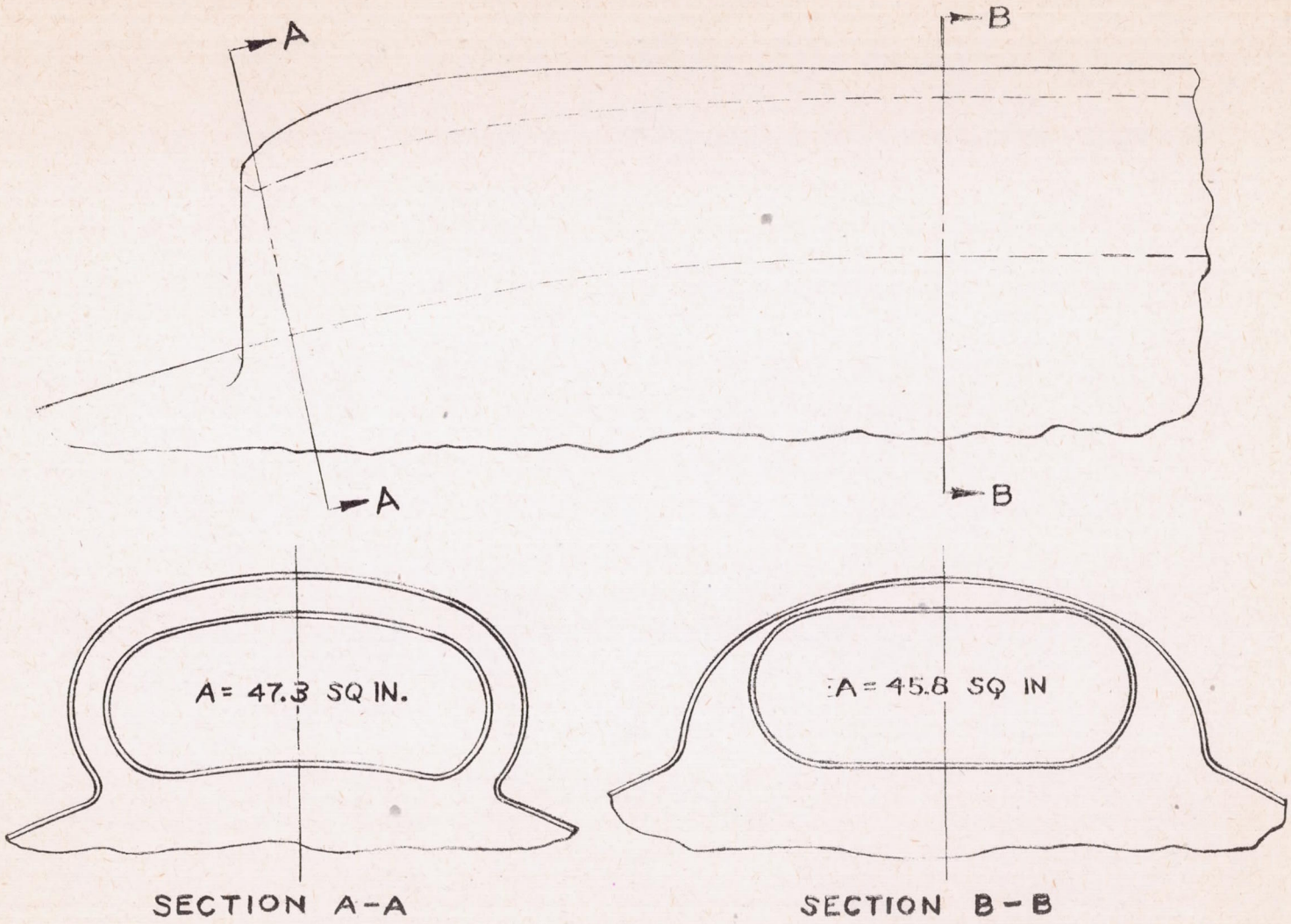

Figure 9.- Carburetor air scoop 3, tested on model A.

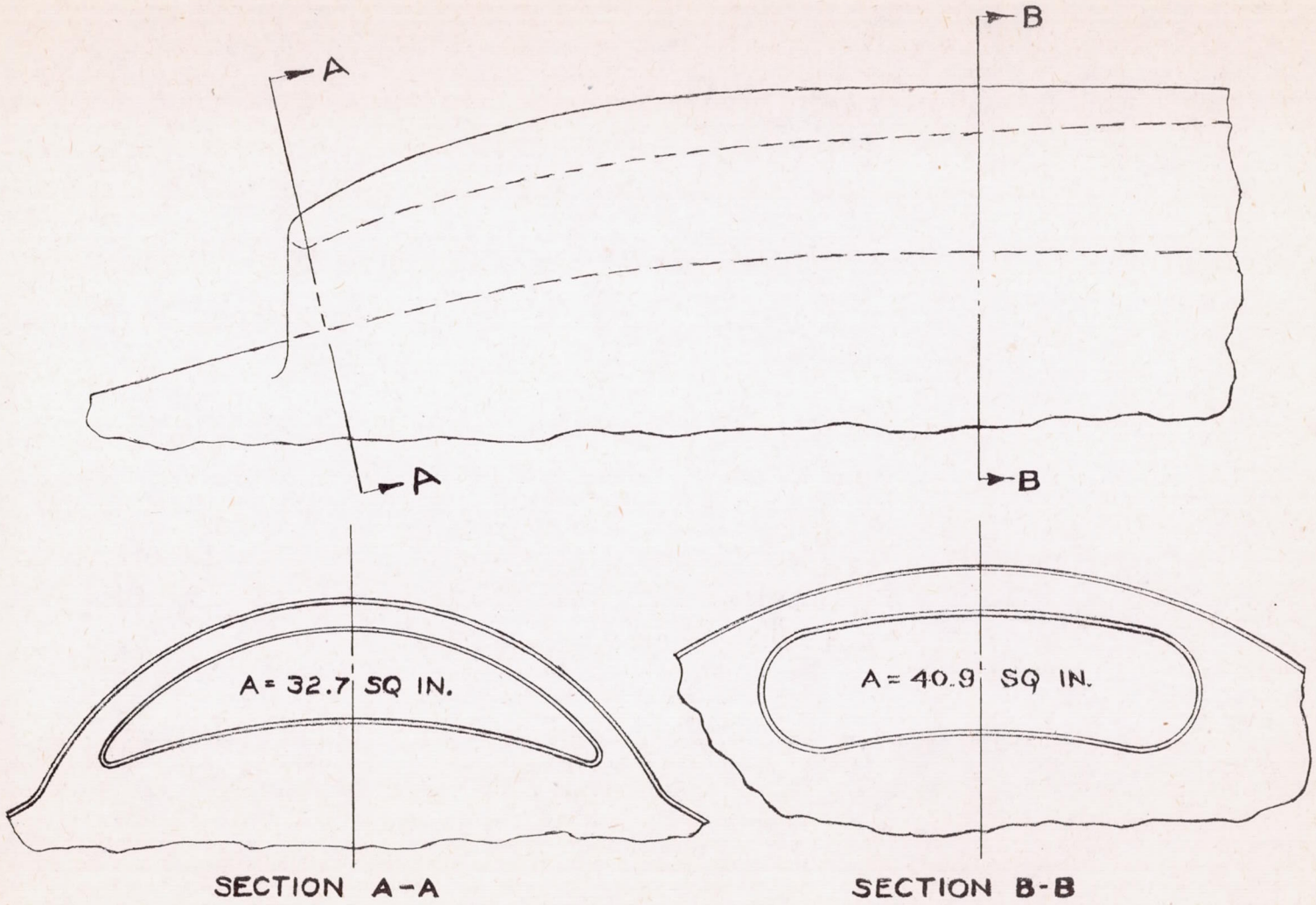

Figure 10.- Carburetor air scoop 4, tested on model A.

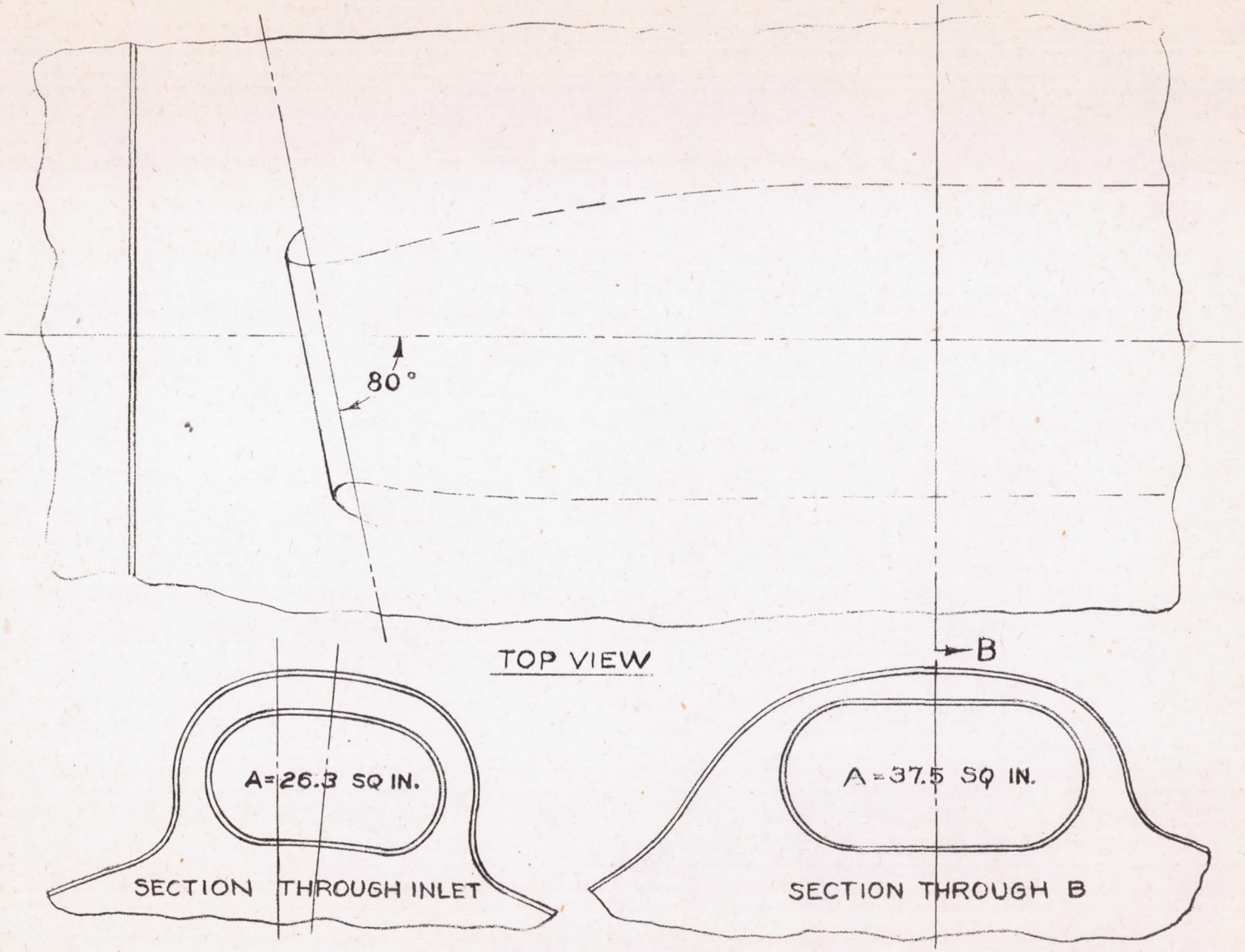

Figure 11.- Carburetor air scoop 5, tested on model A.

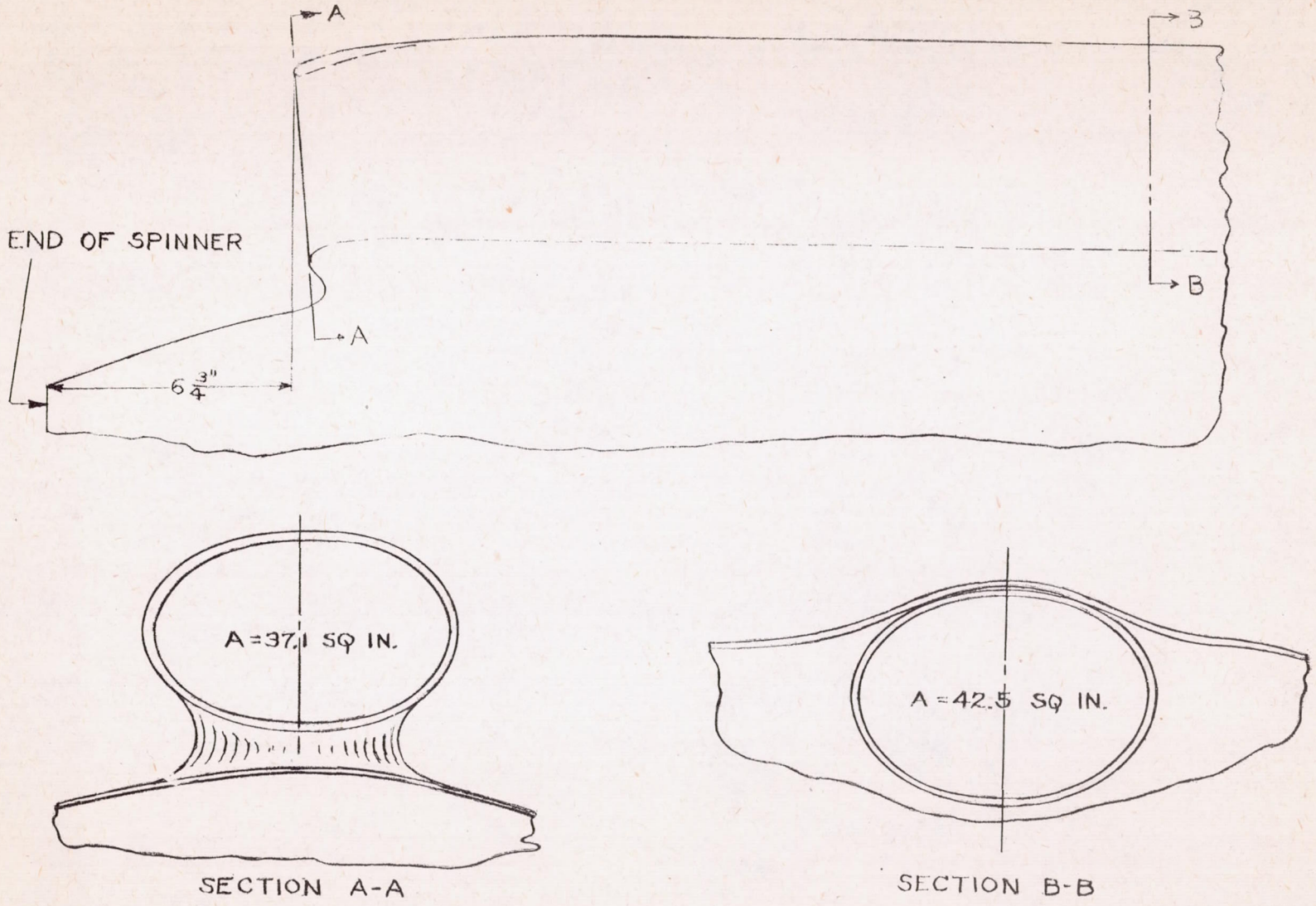

Figure 12.- Carburetor air scoop 6, tested on model B.

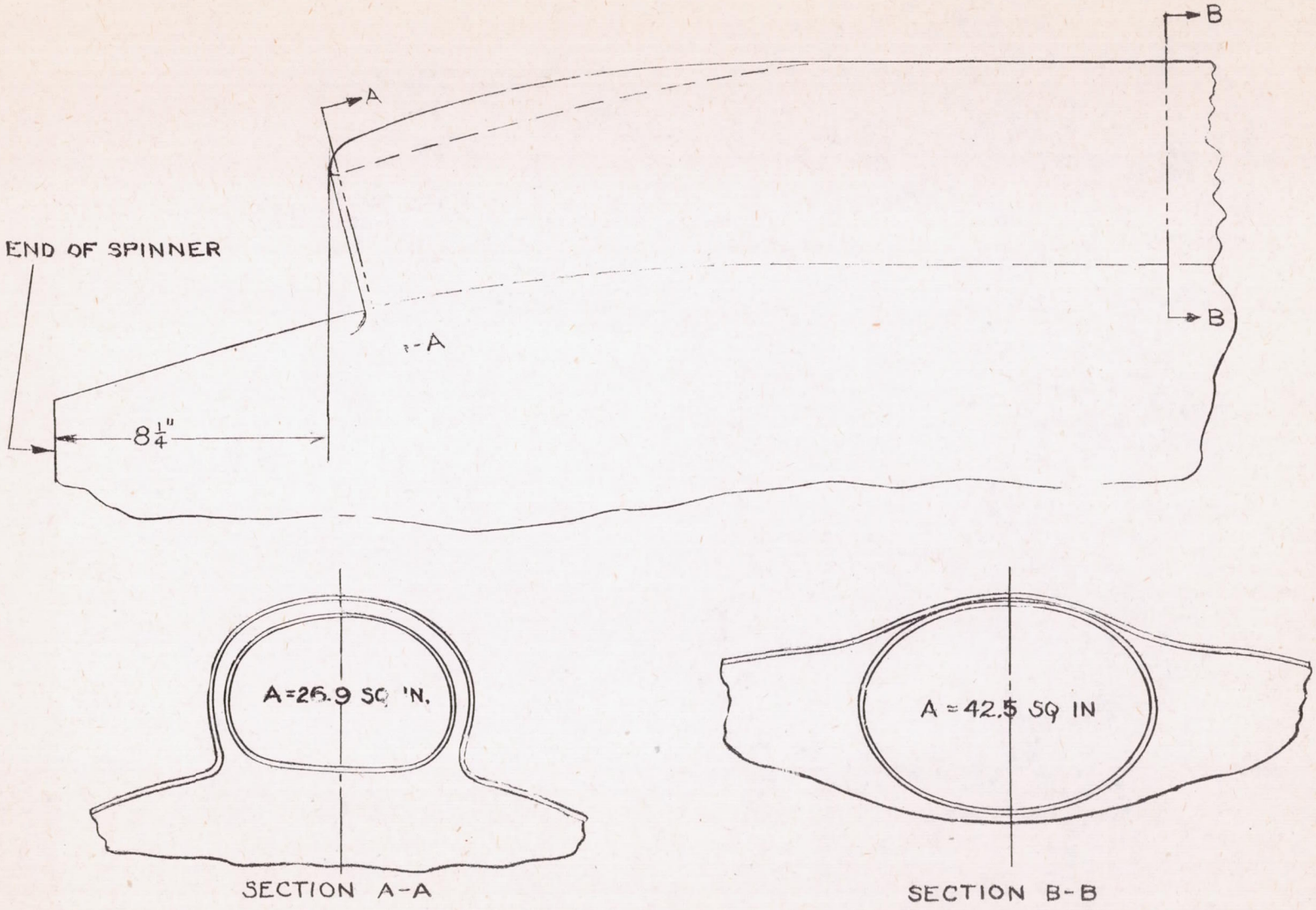

Figure 13.- Carburetor air scoop 7, tested on model B.

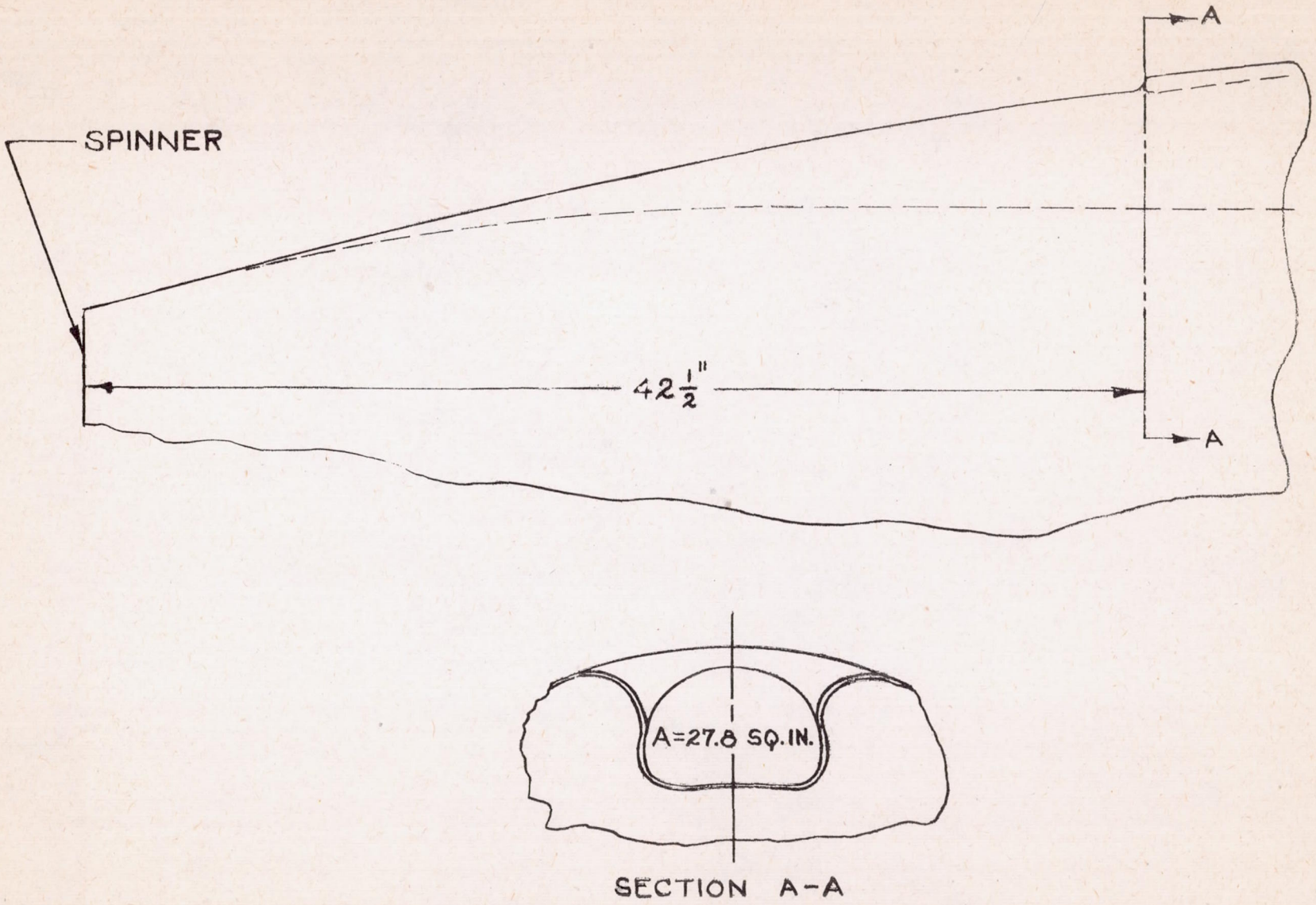

Figure 14.- Carburetor air scoop 8, tested on model B.

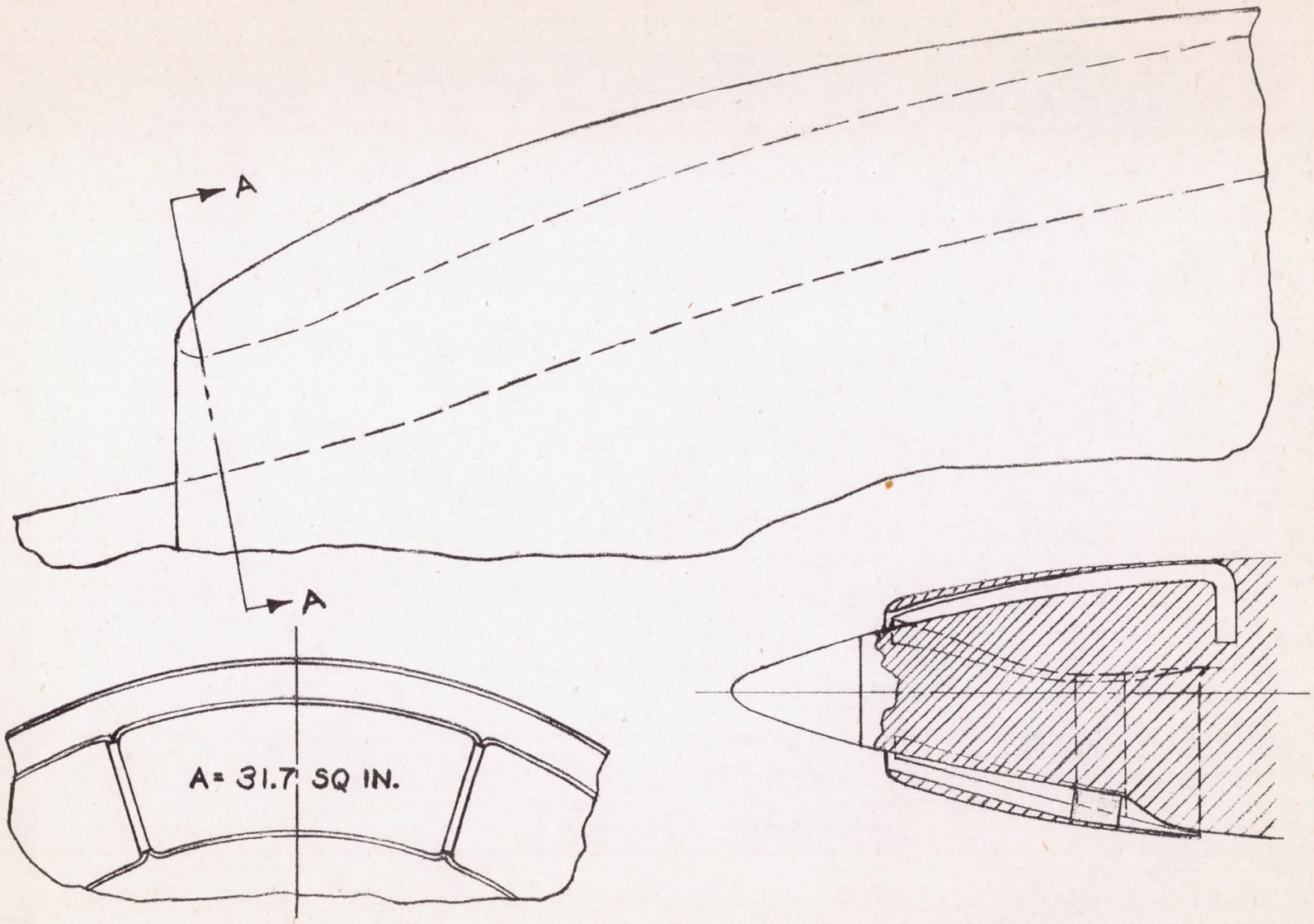

Figure 15.- Carburetor air scoop 9, tested on model A.

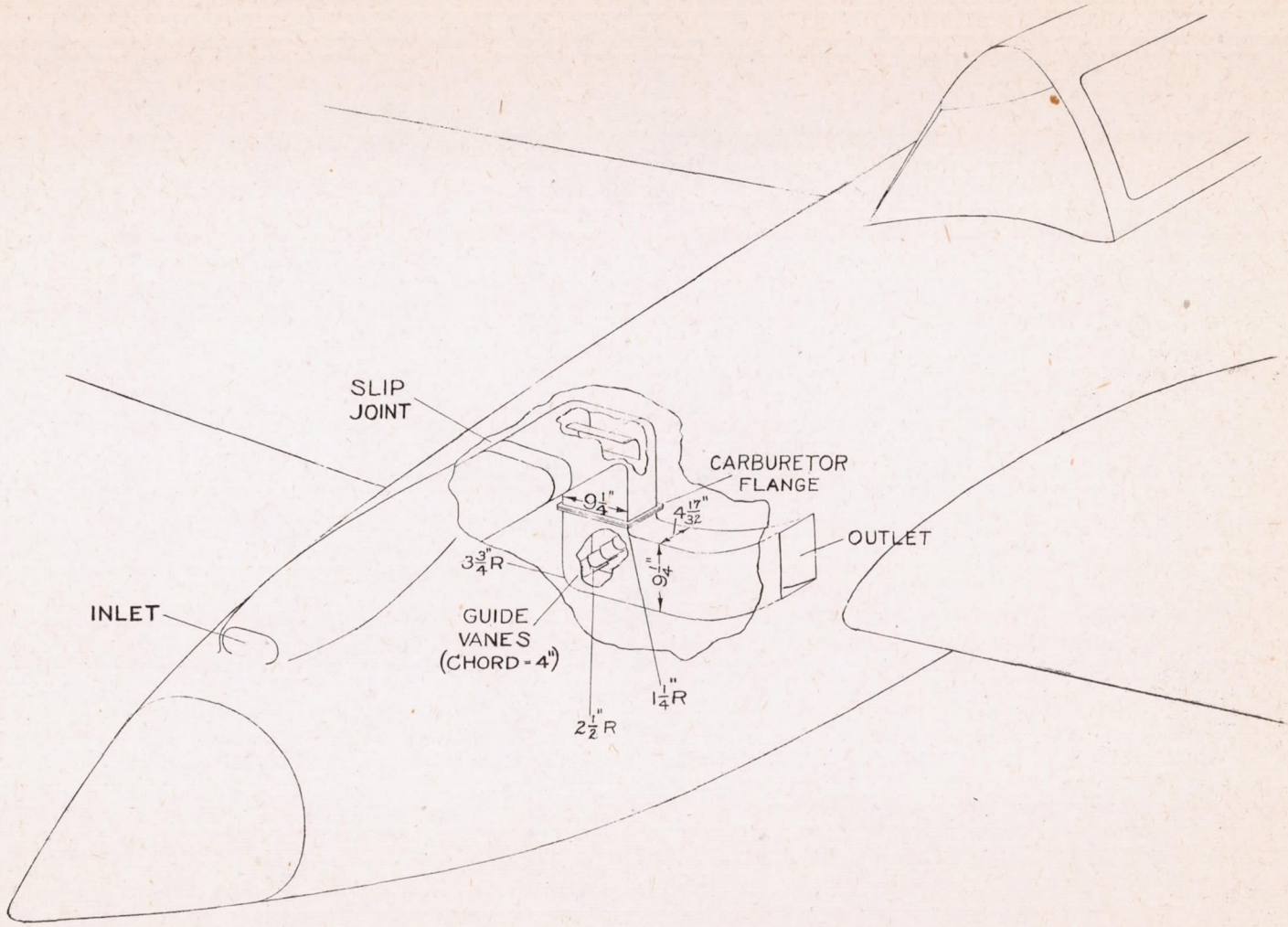

FIGURE 16 – TYPICAL CARBURETOR AIR-SCOOP INSTALLATION ON MODEL A.

NACA

Fig. 17

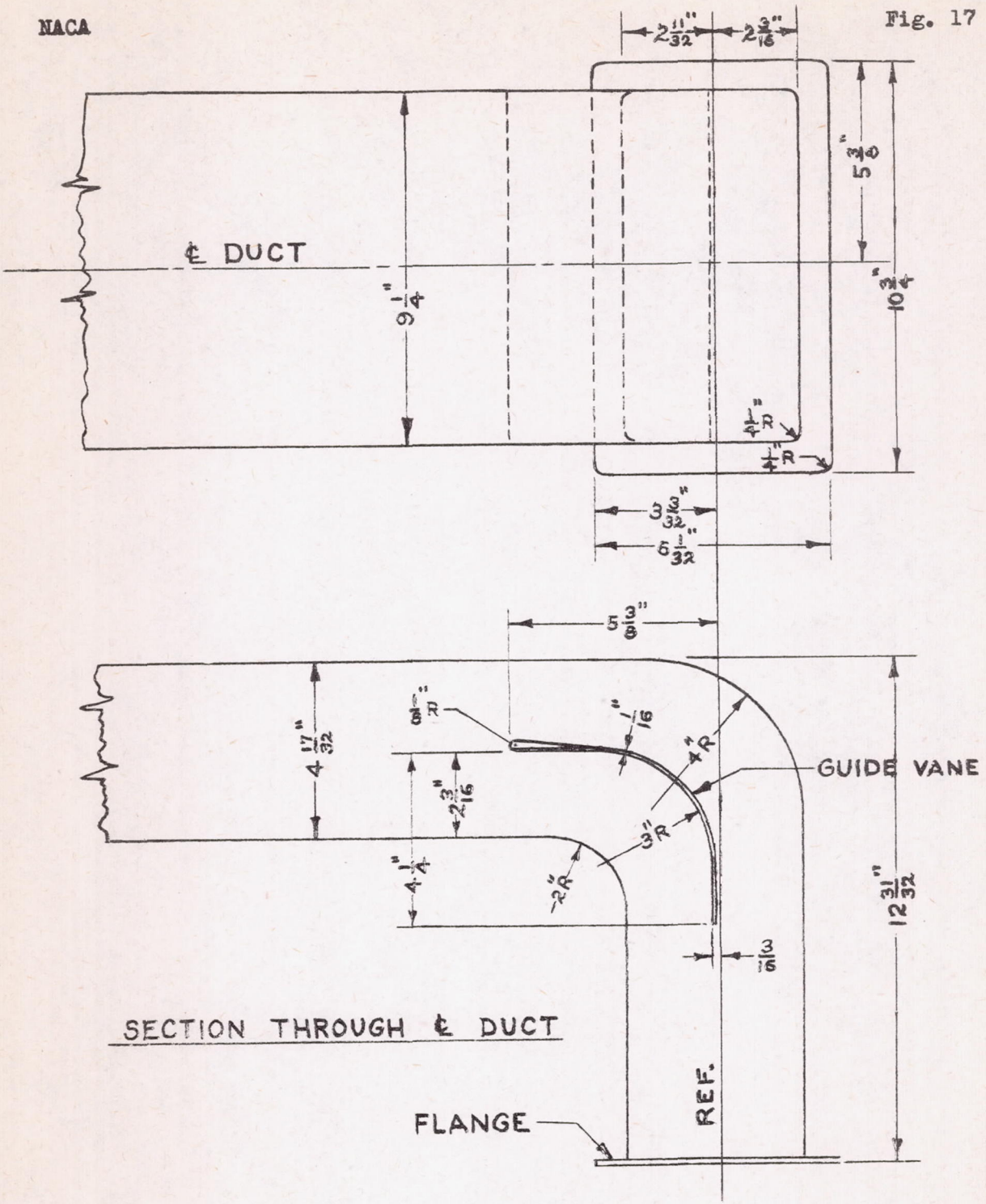

Figure 17.- Dimensions of duct turn ahead of carburetor location on model A.

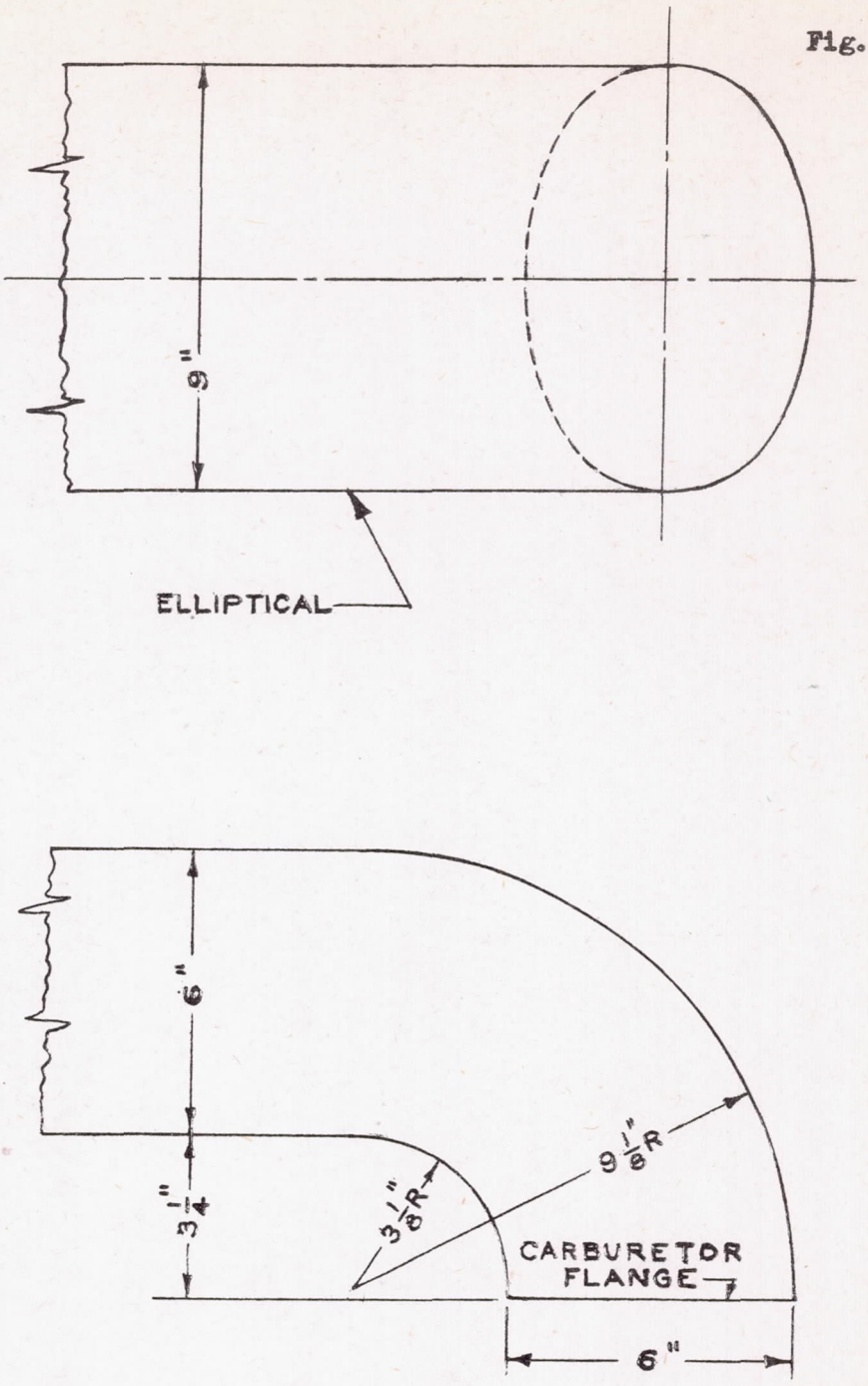

Figure 18.- Dimensions of duct turn ahead of carburetor location on model B.

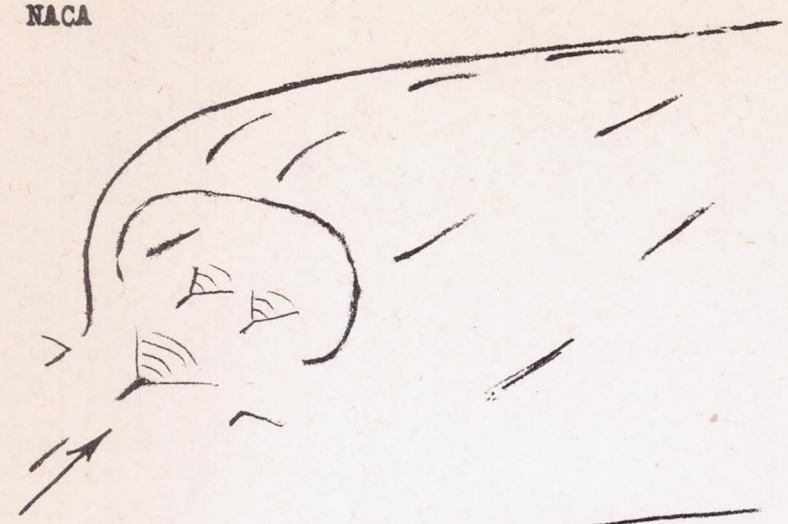

(a) $V_1/V_o = 0.21$.

(b) $V_1/V_o = 0.36$.

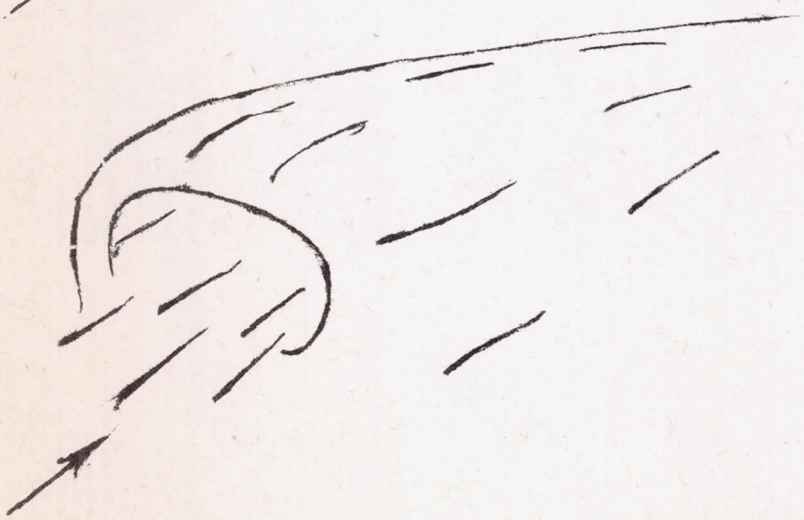

(c) $V_1/V_o = 0.53$.

Figure 19.- Tuft survey showing effect of inlet velocity on flow at inlet of scoop 3; propeller off.

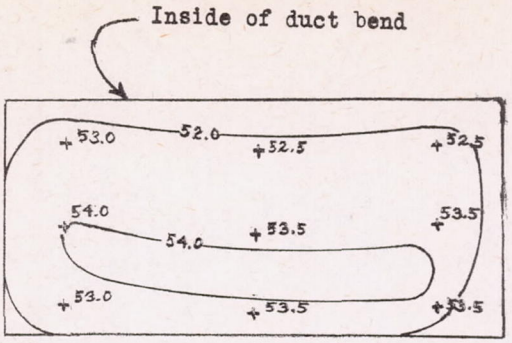

V_i/V_o	Q/V_o	Ram $\%q_o$	q_o mm alcohol
0.34	0.05	91.5	57.8

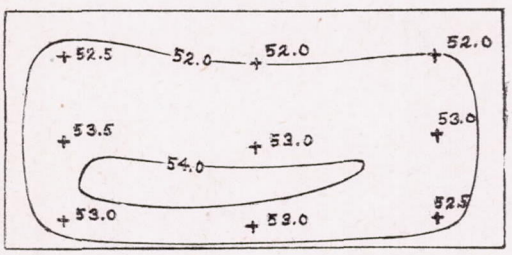

V_i/V_o	Q/V_o	Ram $\%q_o$	q_o mm alcohol
.47	.06	90.7	57.8

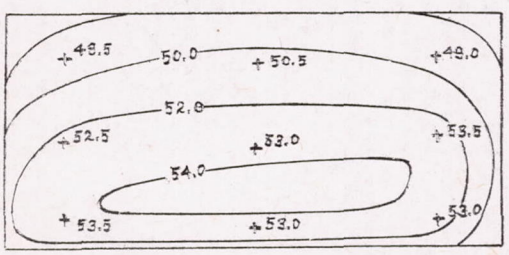

V_i/V_o	Q/V_o	Ram $\%q_o$	q_o mm alcohol
.75	.10	88.5	57.8

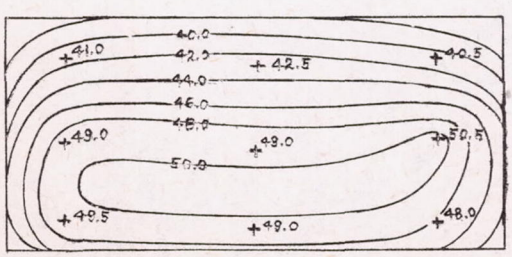

V_i/V_o	Q/V_o	Ram $\%q_o$	q_o mm alcohol
1.13	.16	78.5	57.8

Figure 20.- Effect of V_i/V_o on ram with scoop 1; propeller off, $\alpha = 1^\circ$. Values indicate total pressure, H_c, in millimeters of alcohol.

L-166

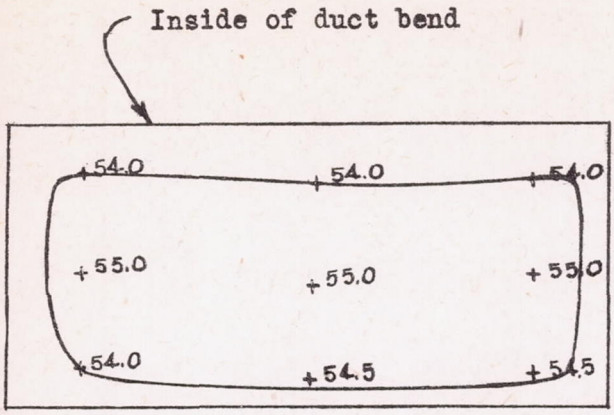

V_i/V_o = 0.32 Ram = 90.8%q_o

Q/V_o = 0.07 q_o = 59.4 mm alcohol

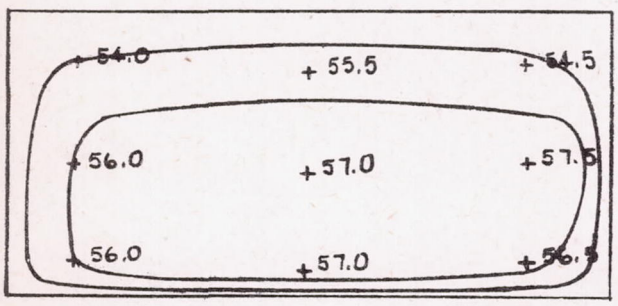

V_i/V_o = 0.45 Ram = 91.6%q_o

Q/V_o = 0.09 q_o = 60.4 mm alcohol

Figure 21.- Effect of V_i/V_o on ram with scoop 2; propeller off, $\alpha = 1^\circ$. Values indicate total pressure, H_c, in millimeters of alcohol.

Inside of duct bend

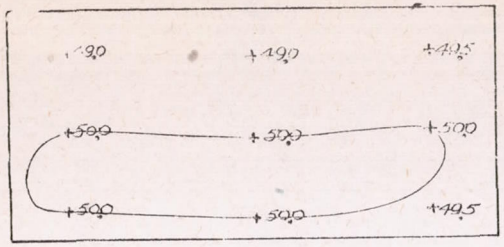

V_i/V_o = 0.21 Ram = 83.7%q_o

Q/V_o = 0.07 q_o = 58.6 mm alcohol

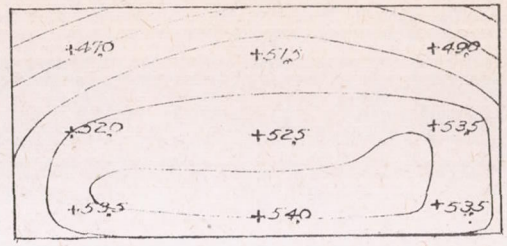

V_i/V_o = 0.43 Ram = 87.5%q_o

Q/V_o = 0.14 q_o = 58.4 mm alcohol.

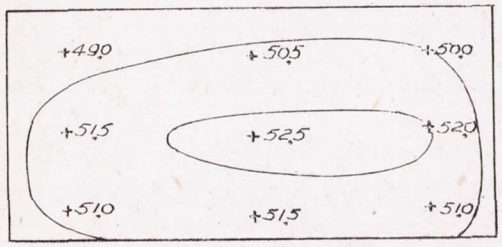

V_i/V_o = 0.31 Ram = 86.7%q_o

Q/V_o = 0.10 q_o = 58.0 mm alcohol

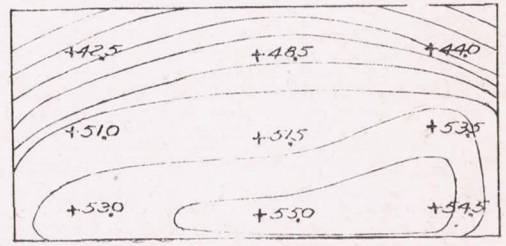

V_i/V_o = 0.50 Ram = 84.3%q_o

Q/V_o = 0.17 q_o = 57.8 mm alcohol

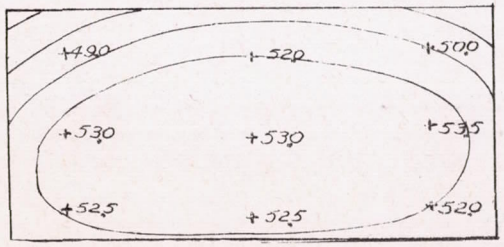

V_i/V_o = 0.37 Ram = 88.2%

Q/V_o = 0.12 q_o = 58.2 mm alcohol

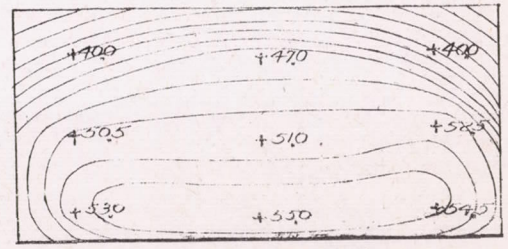

V_i/V_o = 0.53 Ram = 82.2%q_o

Q/V_o = 0.17 q_o = 57.8 mm alcohol

Figure 22.- Effect of V_i/V_o on ram with scoop 3; propeller off, $\alpha = 1^\circ$. Values indicate total pressure, H_c, in millimeters of alcohol.

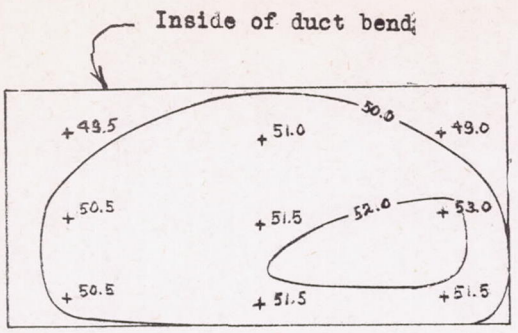

$\frac{V_i}{V_o}$	$\frac{Q}{V_o}$	Ram $\%q_o$	q_o mm alcohol
0.27	0.06	87.8	57.3

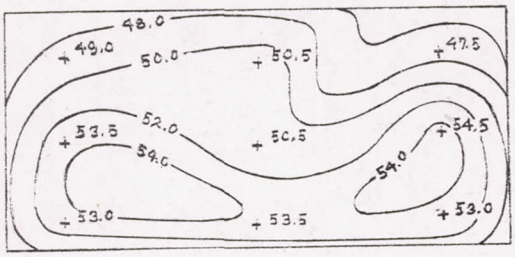

.44	.10	89.3	57.3

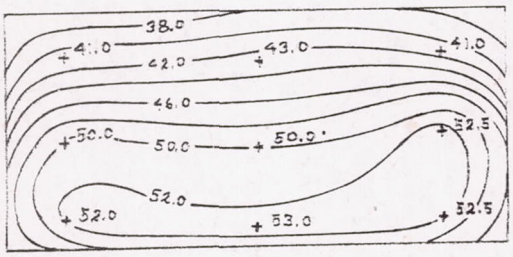

.69	.16	82.2	57.3

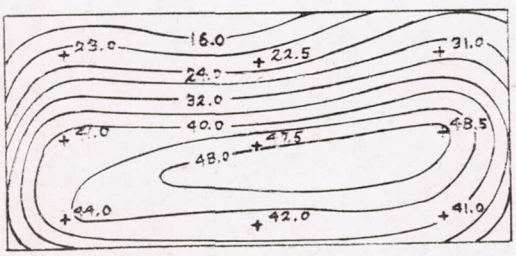

.90	.20	57.1	57.3

Figure 23.- Effect of V_i/V_o on ram with scoop 4; propeller off, $\alpha = 1^\circ$. Values indicate total pressure, H_c, in millimeters of alcohol.

L-166

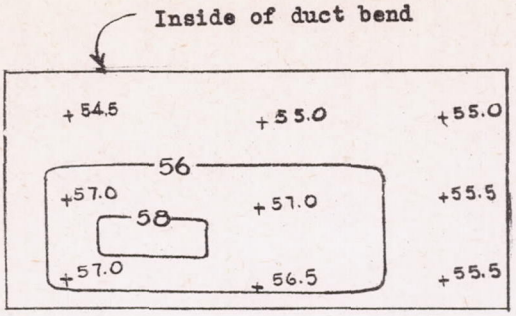

$\frac{V_i}{V_o}$	$\frac{Q}{V_o}$	Ram %	q_o mm alcohol
0.87	0.07	91.3	60.0

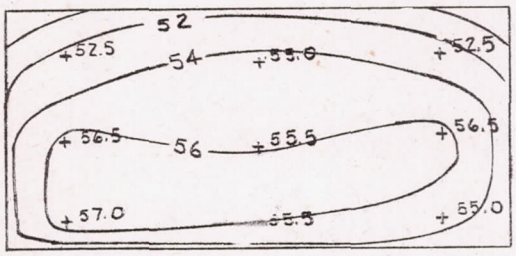

.54	.10	91.0	60.5

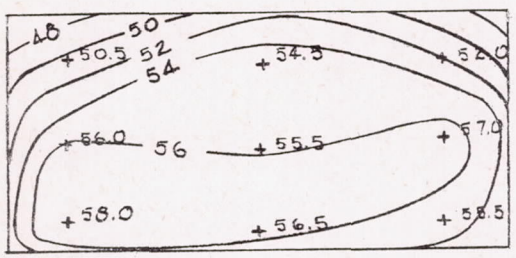

.61	.11	91.0	60.5

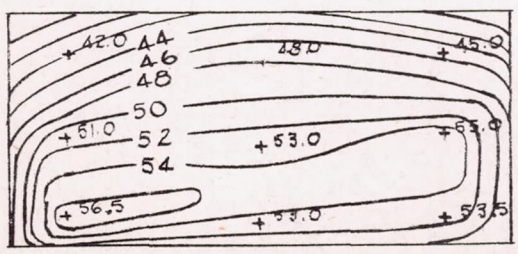

.87	.16	83.0	59.9

Figure 24.- Effect of V_i/V_o on ram with scoop 5, propeller off, $\alpha = 1^\circ$. Values indicate total pressure, H_c, in millimeters of alcohol.

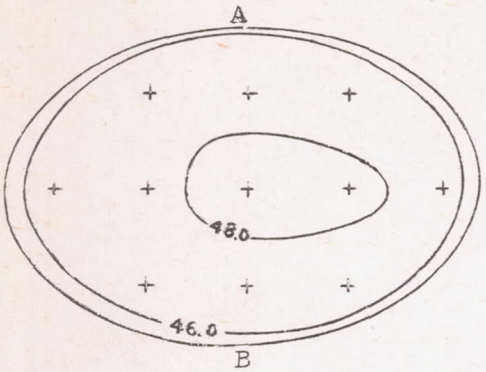

(a) Scoop 6.

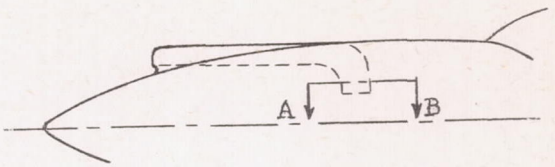

V_i/V_o = 0.40 Ram = 96.0%q_o

Q/V_o = 0.10 q_o = 49.0 mm alcohol

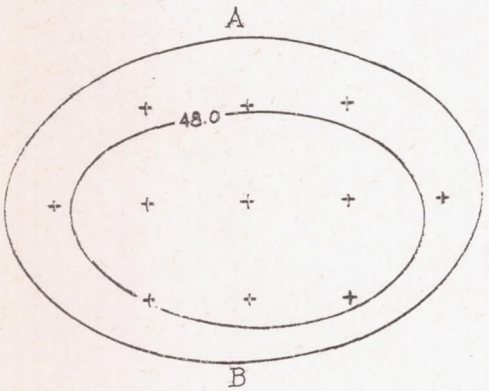

(b) Scoop 7.

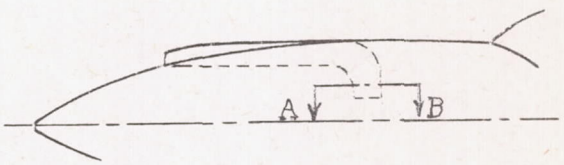

V_i/V_o = 0.40 Ram = 98.0%q_o

Q/V_o = 0.08 q_o = 48.6 mm alcohol

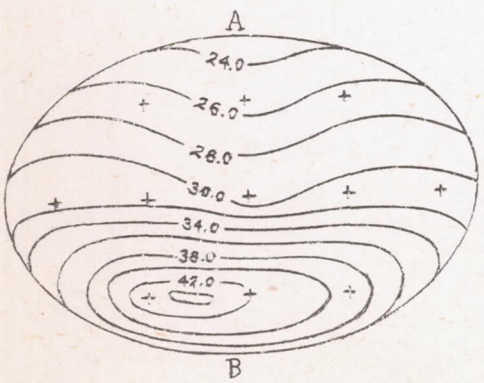

(c) Scoop 8.

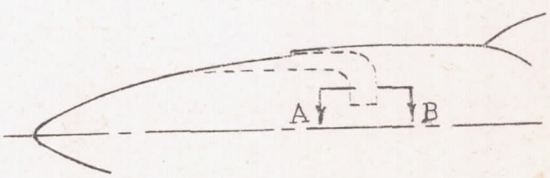

V_i/V_o = 0.40 Ram = 73.5%q_o

Q/V_o = 0.08 q_o = 49.0 mm alcohol

Figure 25.- Effect of inlet position on ram. Contour values indicate total pressure, H_c, in millimeters of alcohol; propeller off, $\alpha = 1^\circ$.

Inside of duct bend

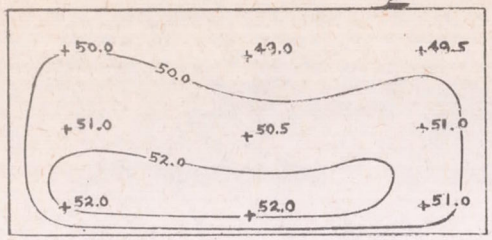

V_i/V_o = 0.23 Ram = 86.8%q_o

Q/V_o = 0.05 q_o = 57.6 mm alcohol
α = 1°

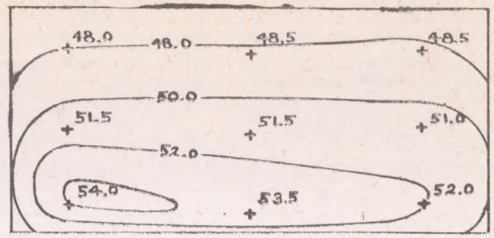

V_i/V_o = 0.52 Ram = 86.0%q_o

Q/V_o = 0.11 q_o = 58.4 mm alcohol
α = 1°

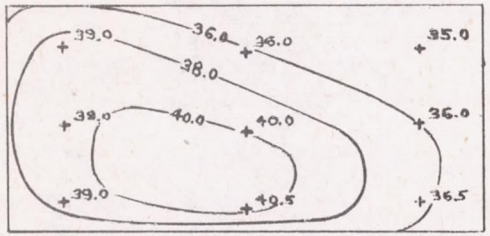

V_i/V_o = 0.22 Ram = 65.6%q_o

Q/V_o = 0.05 q_o = 56.7 mm alcohol
α = 6°

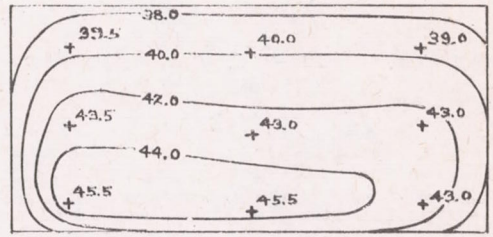

V_i/V_o = 0.57 Ram = 71.0%q_o

Q/V_o = 0.13 q_o = 57.5 mm alcohol
α = 6°

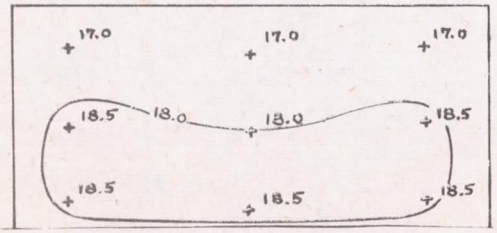

V_i/V_o = 0.29 Ram = 30.6%q_o

Q/V_o = 0.07 q_o = 56.2 mm alcohol
α = 12°

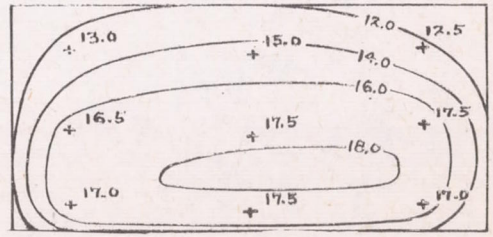

V_i/V_o = 0.55 Ram = 27.8%q_o

Q/V_o = 0.12 q_o = 56.4 mm alcohol
α = 12°

Figure 26.- Distribution of total pressure, H_c, with scoop 9; propeller off. Values of H_c are in millimeters of alcohol.

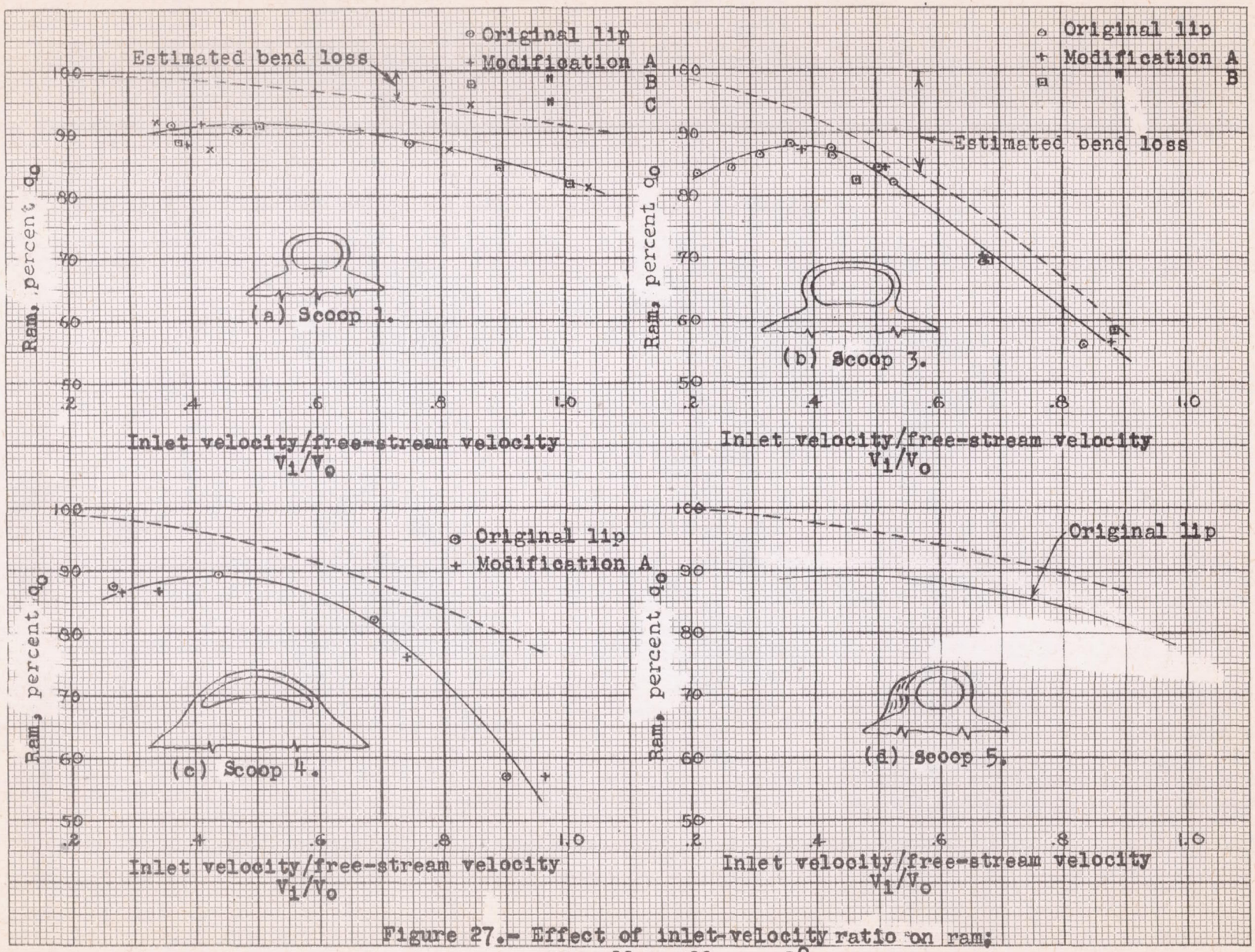

Figure 27.- Effect of inlet-velocity ratio on ram; propeller off, $\alpha = 1^\circ$.

L-166

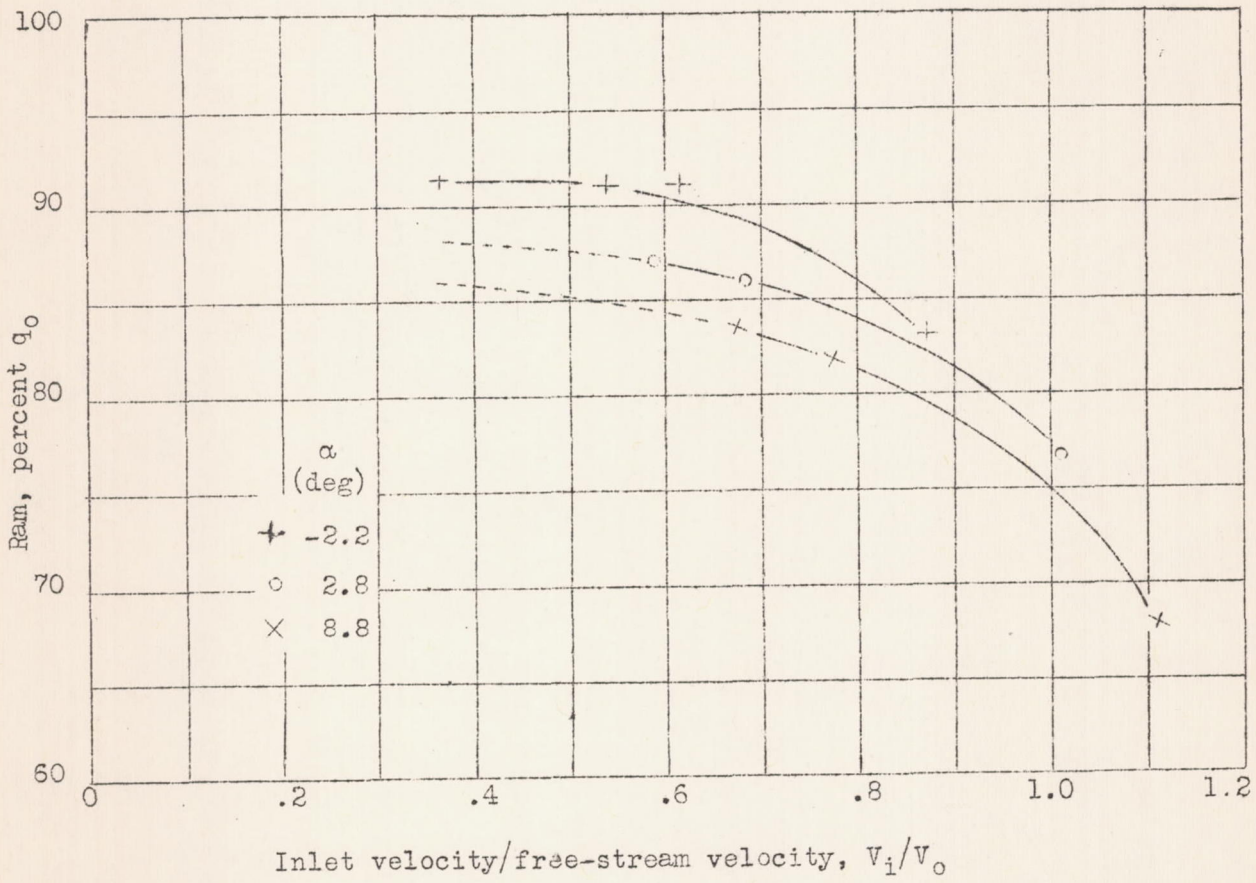

Figure 28.- Effect of angle of attack on ram; scoop 5, propeller off.

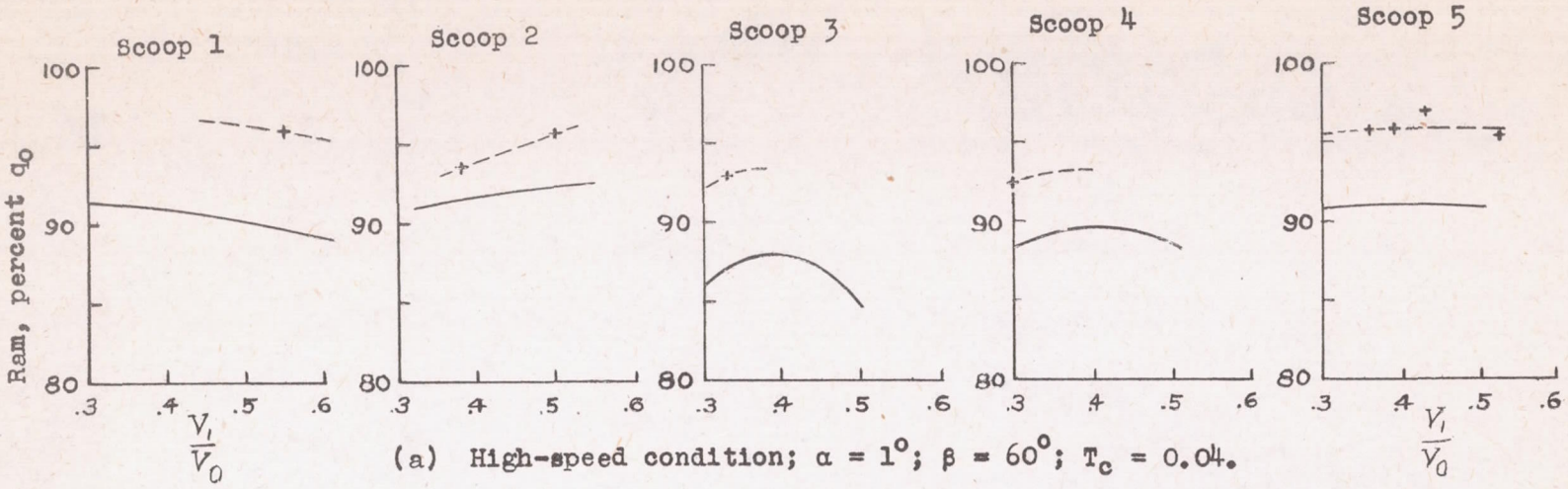

(a) High-speed condition; $\alpha = 1^\circ$; $\beta = 60^\circ$; $T_c = 0.04$.

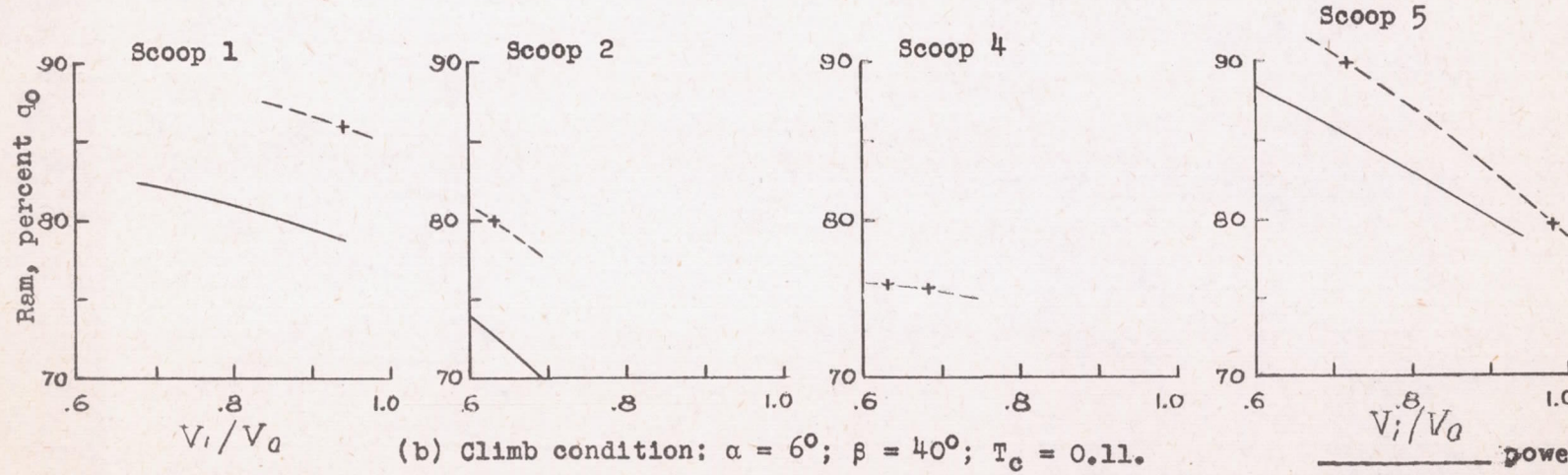

(b) Climb condition: $\alpha = 6^\circ$; $\beta = 40^\circ$; $T_c = 0.11$.

Figure 29.- Effect of slipstream on ram at the carburetor.

Scoop 5

Inside of duct bend

Scoop 2

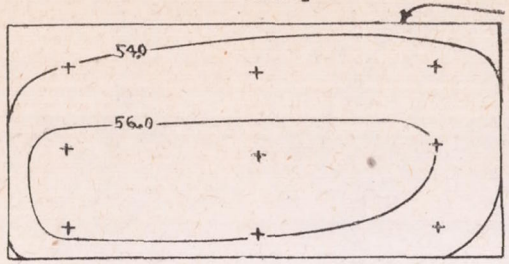

V_i/V_o = 0.40 Ram = 91.2%q_o
Q/V_o = 0.07 q_o = 60.1 mm alcohol
α = 1° propeller off

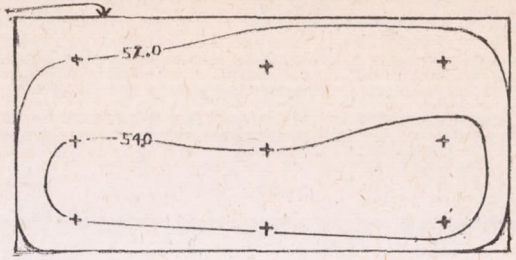

V_i/V_o = 0.40 Ram = 91.0%q_o
Q/V_o = 0.08 q_o = 59.5 mm alcohol
α = 1° propeller off

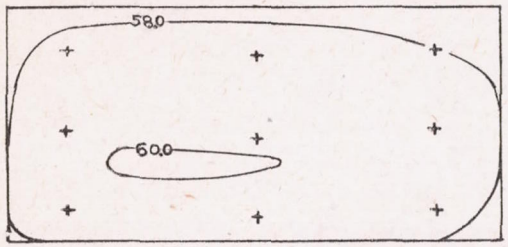

V_i/V_o = 0.40 Ram = 96.3%q_o
Q/V_o = 0.07 q_o = 60.3 mm alcohol
α = 1° β = 60° T_c = 0.04

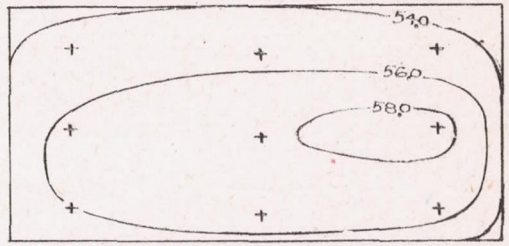

V_i/V_o = 0.40 Ram = 93.8%q_o
Q/V_o = 0.08 q_o = 59.3 mm alcohol
α = 1° β = 60° T_c = 0.04

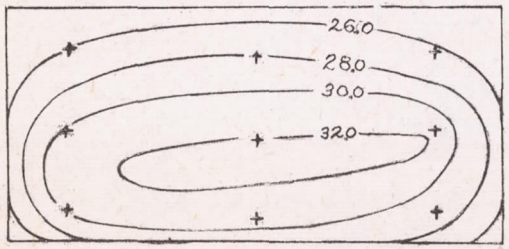

V_i/V_o = 0.80 Ram = 86.9%q_o
Q/V_o = 0.15 q_o = 31.7 mm alcohol
α = 6° β = 40° T_c = 0.11

Figure 30.- Effect of slipstream on total pressure, H_c, with straight and twisted scoops. Values on contours are in millimeters of alcohol.

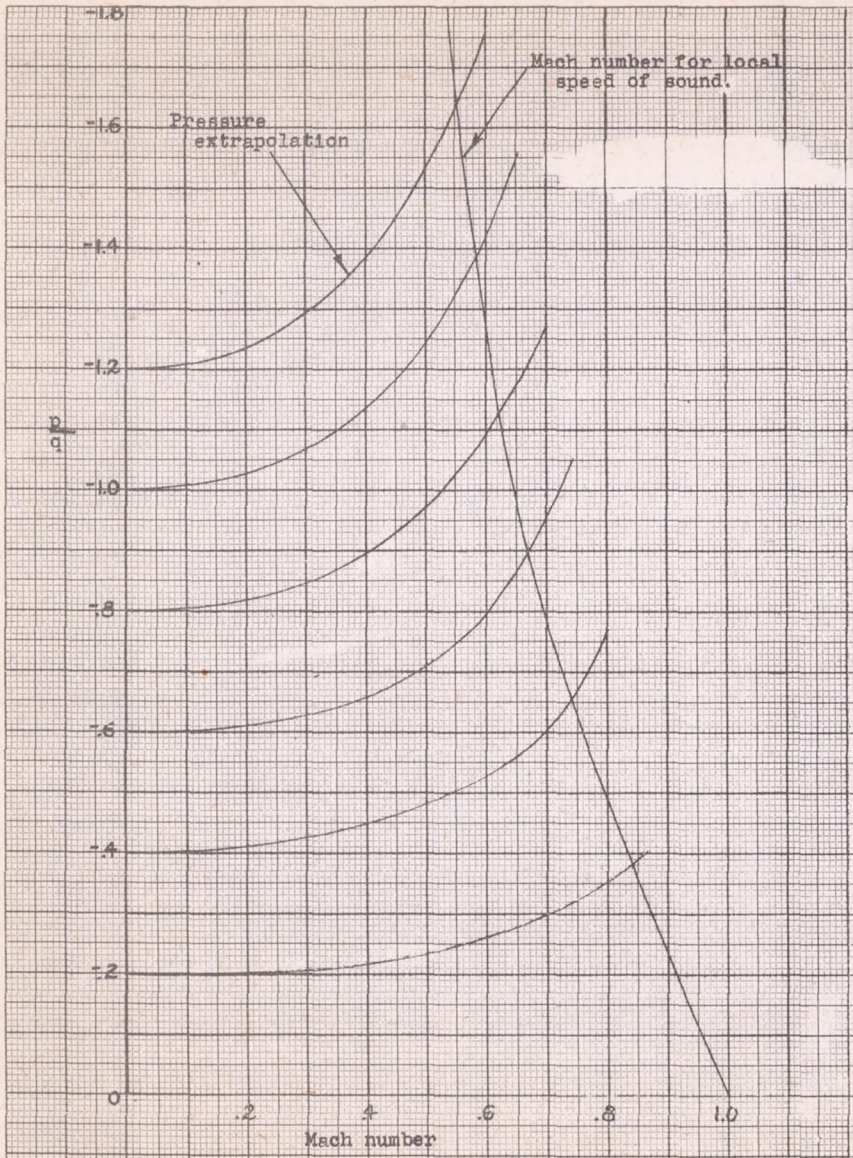

Figure 31.- Pressure coefficient against Mach number for determining critical speed.

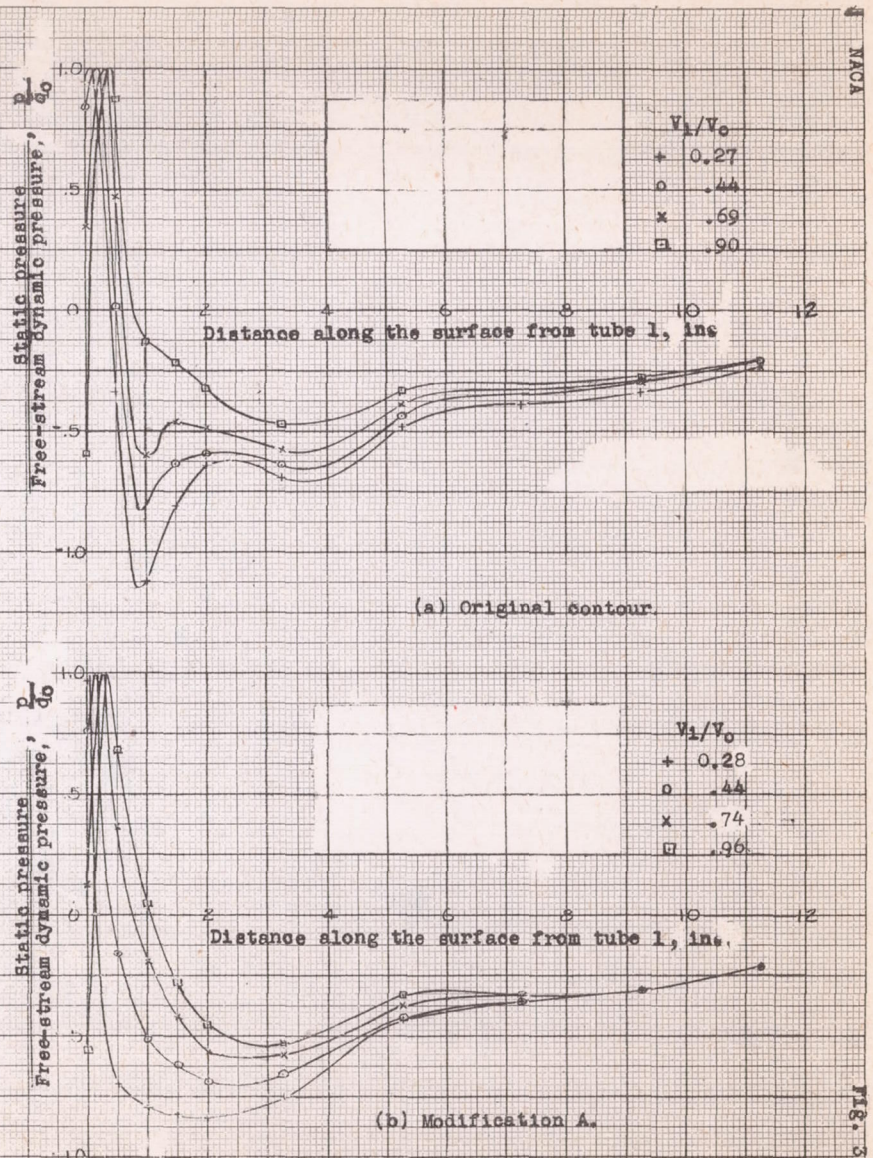

Figure 39.- Effect of inlet-velocity ratio on surface pressure; scoop 4, propeller off; $\alpha = 1^\circ$; Mach number 0.06.

L-166

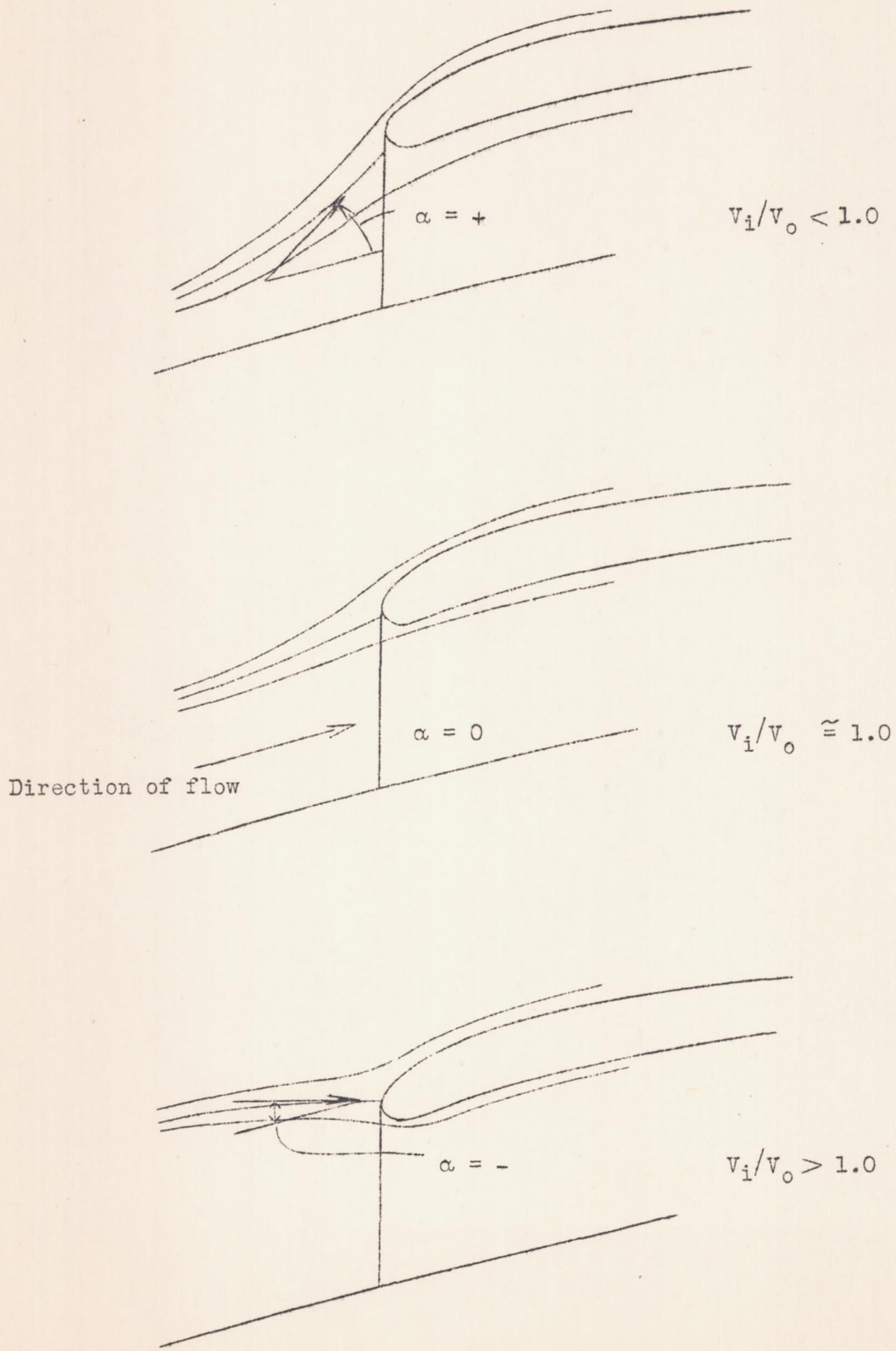

Figure 32.- Effect of V_i/V_o on the angle of attack of the inlet lip.

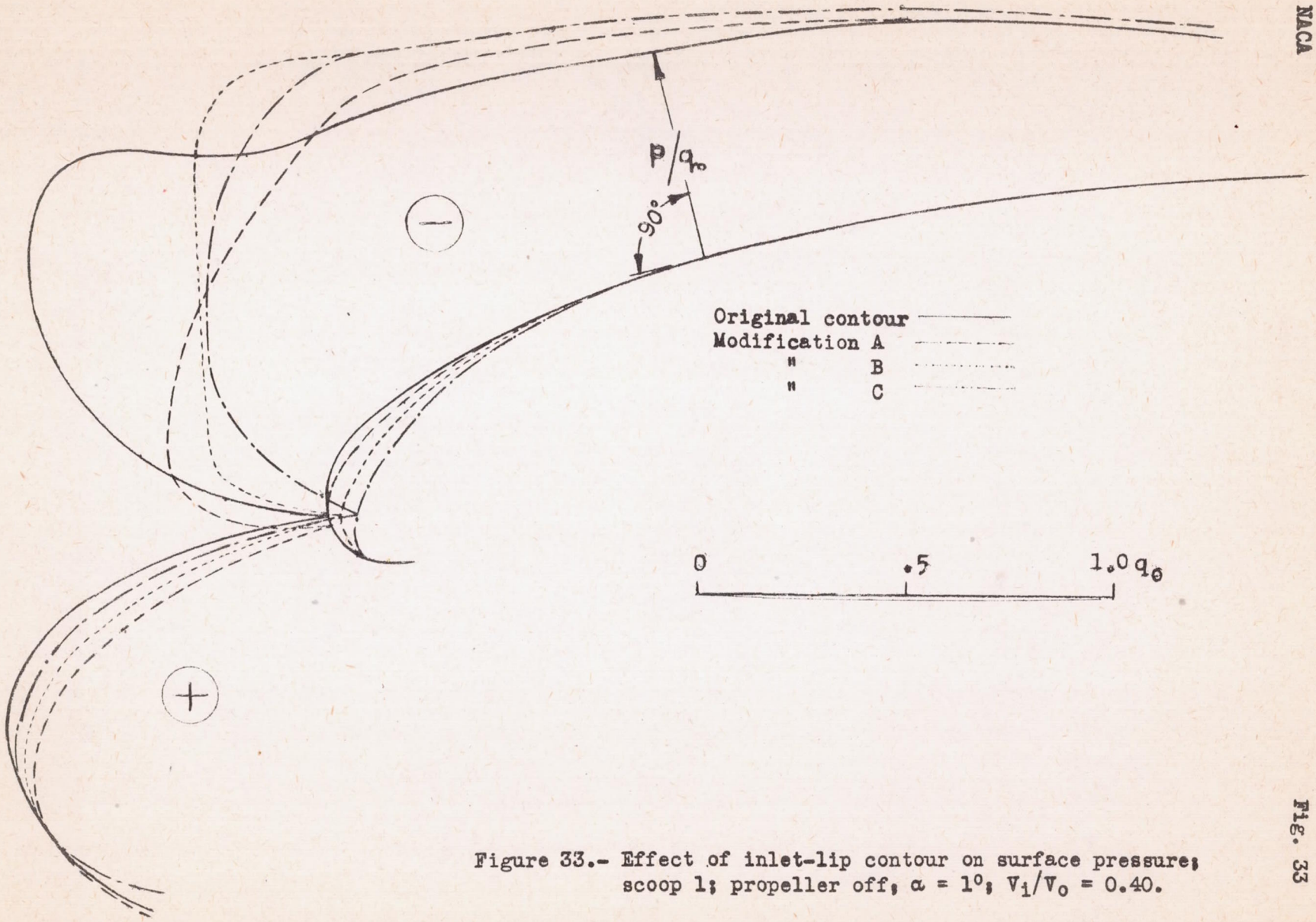

Figure 33.- Effect of inlet-lip contour on surface pressure; scoop 1; propeller off; $\alpha = 1^{\circ}$; $V_i/V_o = 0.40$.

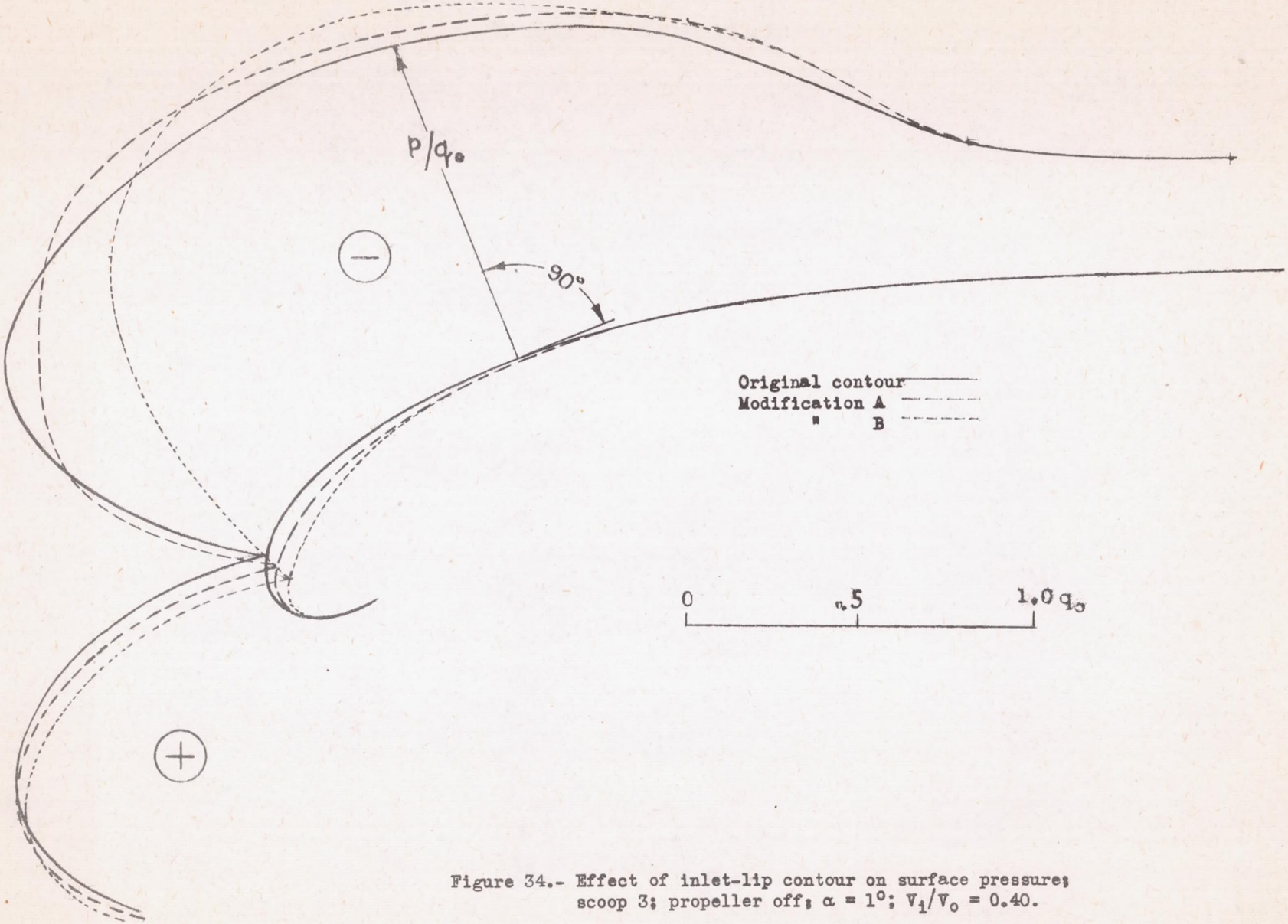

Figure 34.- Effect of inlet-lip contour on surface pressure; scoop 3; propeller off; $\alpha = 1^{\circ}$; $V_i/V_o = 0.40$.

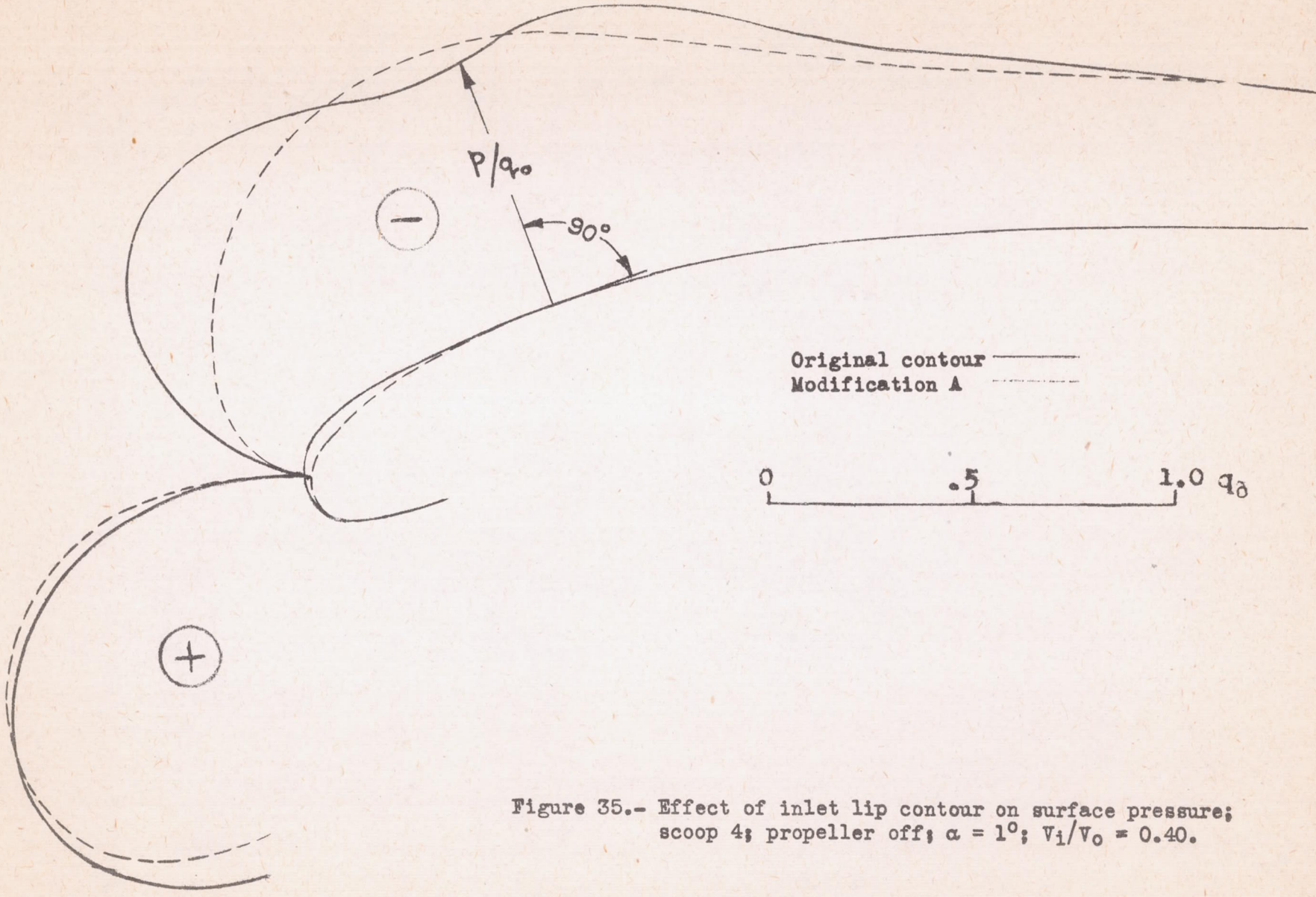

Figure 35.- Effect of inlet lip contour on surface pressure; scoop 4; propeller off; $\alpha = 1^{\circ}$; $V_i/V_o = 0.40$.

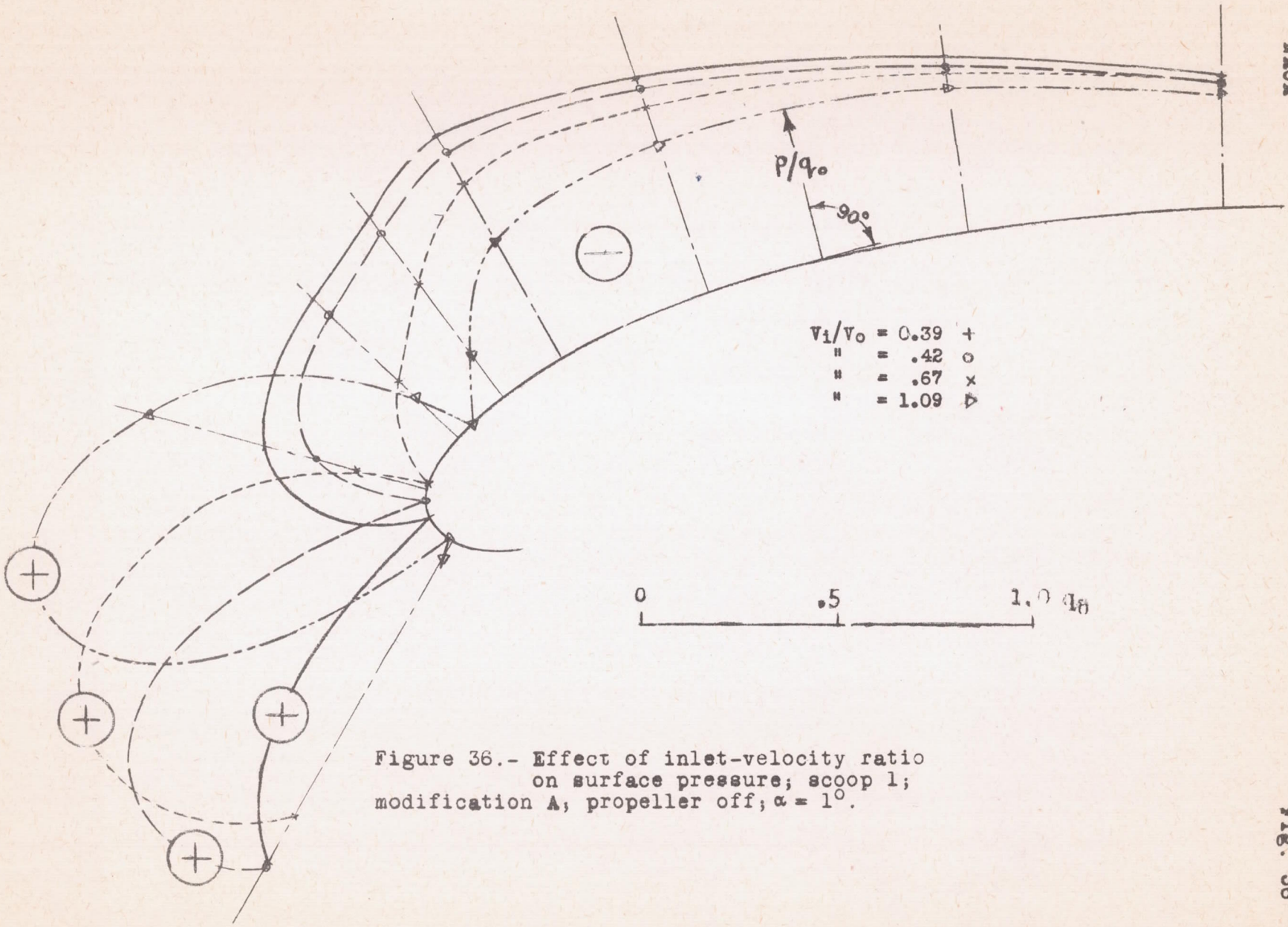

Figure 36.- Effect of inlet-velocity ratio on surface pressure; scoop 1; modification A; propeller off; $\alpha = 1^{\circ}$.

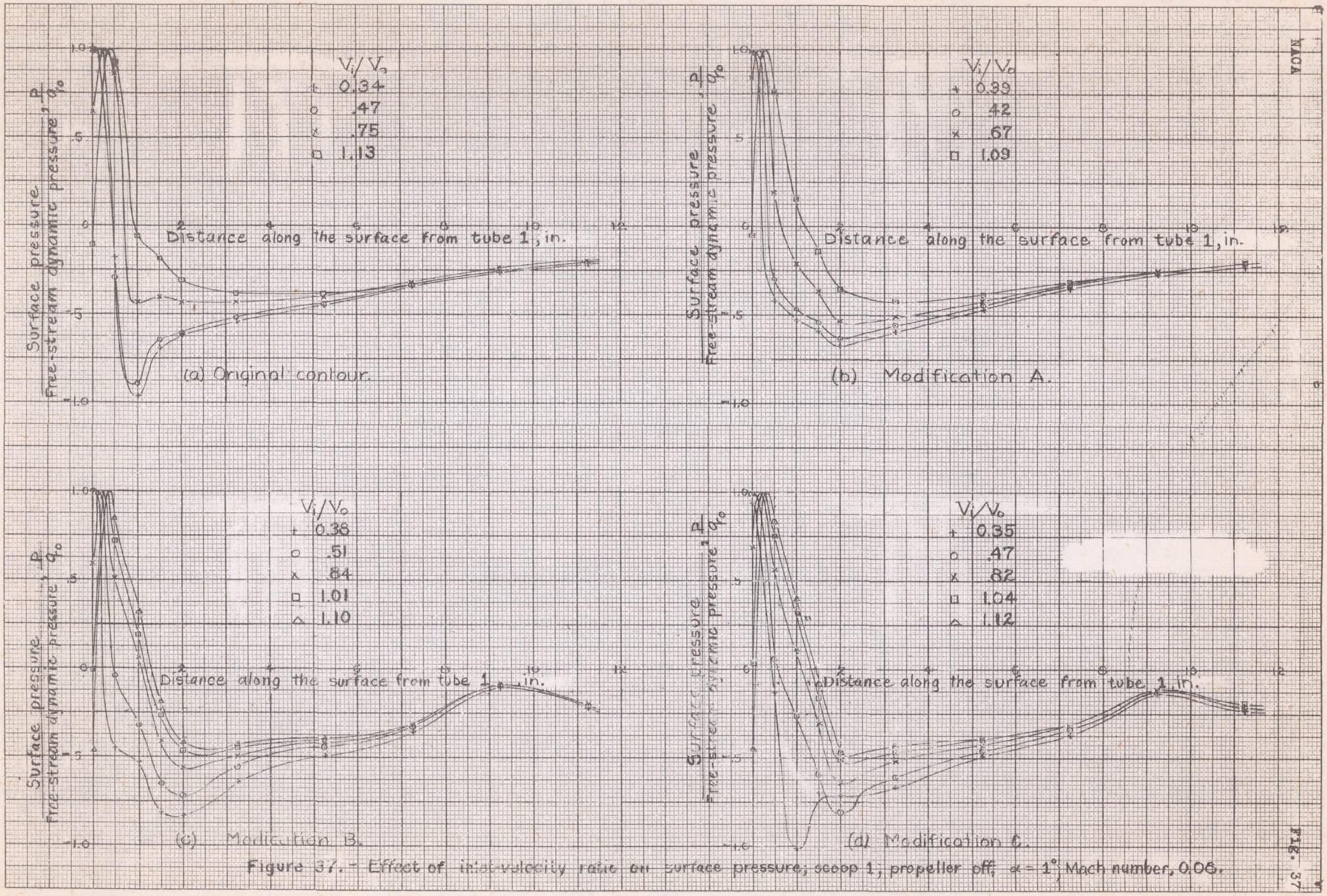

Figure 37.- Effect of inlet-velocity ratio on surface pressure; scoop 1, propeller off, $\alpha = 1°$, Mach number, 0.06.

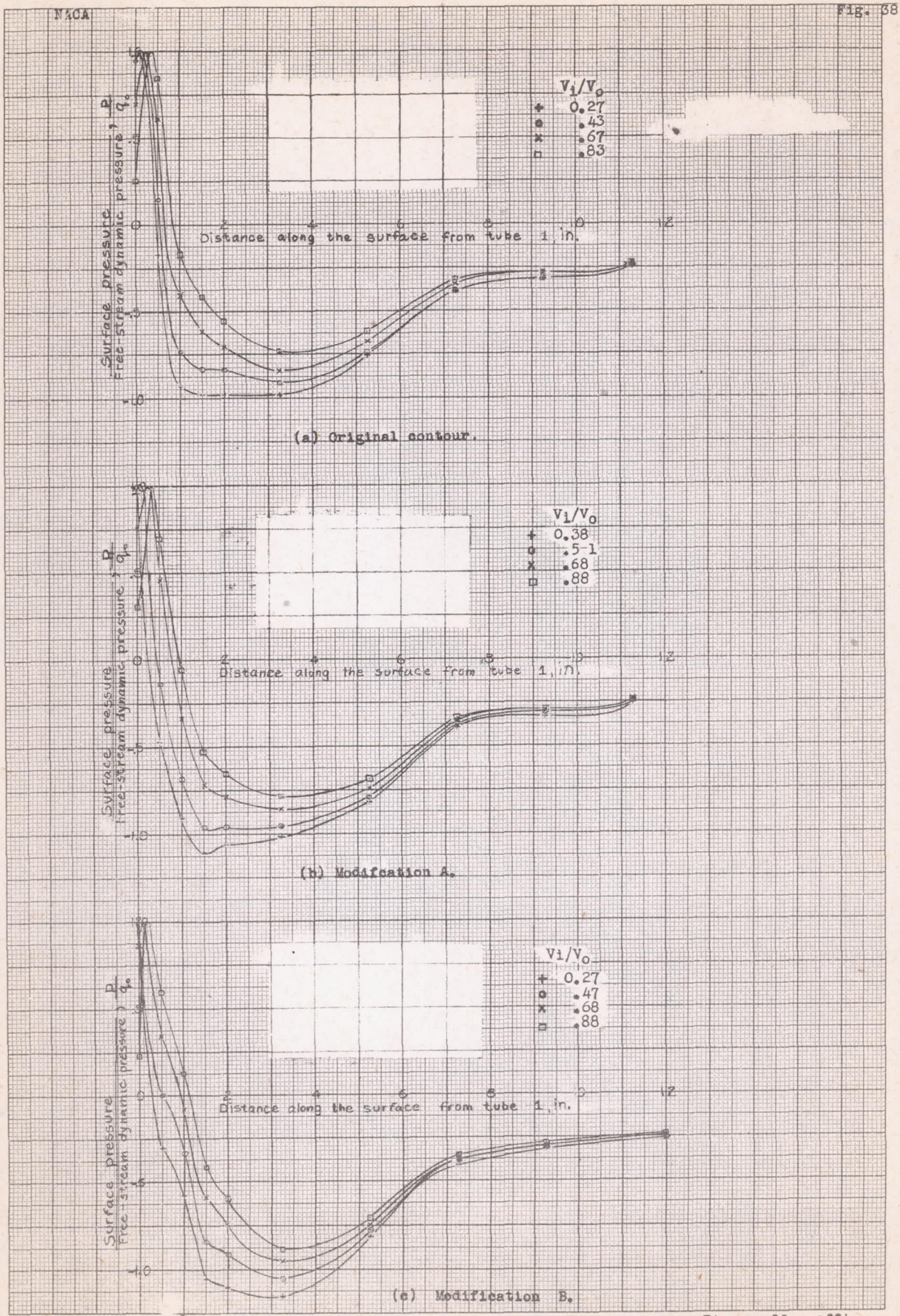

Figure 38. Effect of inlet-velocity ratio on surface pressure; scoop 3; propeller off; $\alpha = 1^{\circ}$; Mach number, 0.08.

"Page missing from available version"

Figure 39

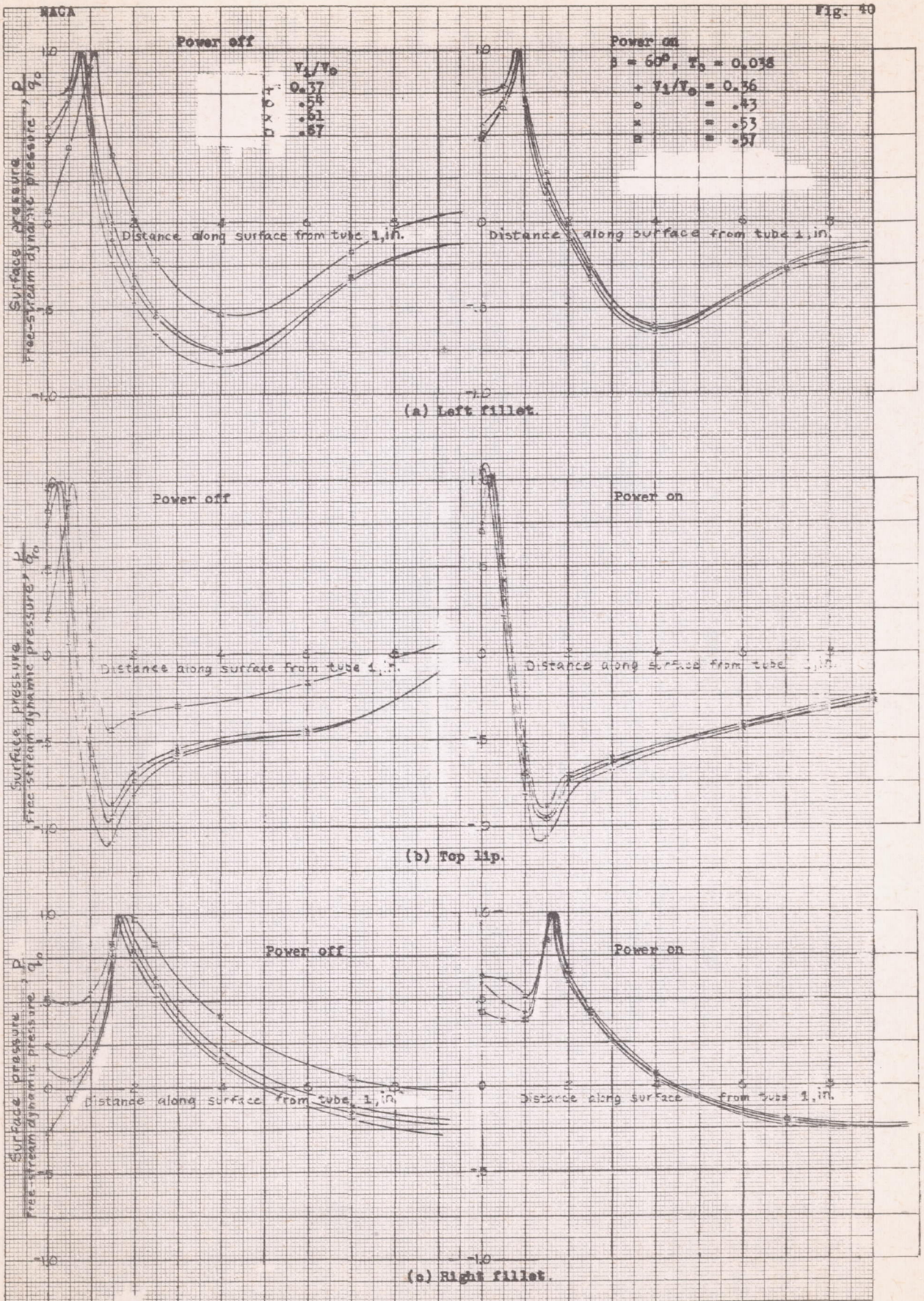

Figure 40.- Effect of inlet-velocity ratio and propeller slipstream on surface pressure; scoop 5, $\alpha = 1^0$; high-speed condition; Mach number, 0.08.

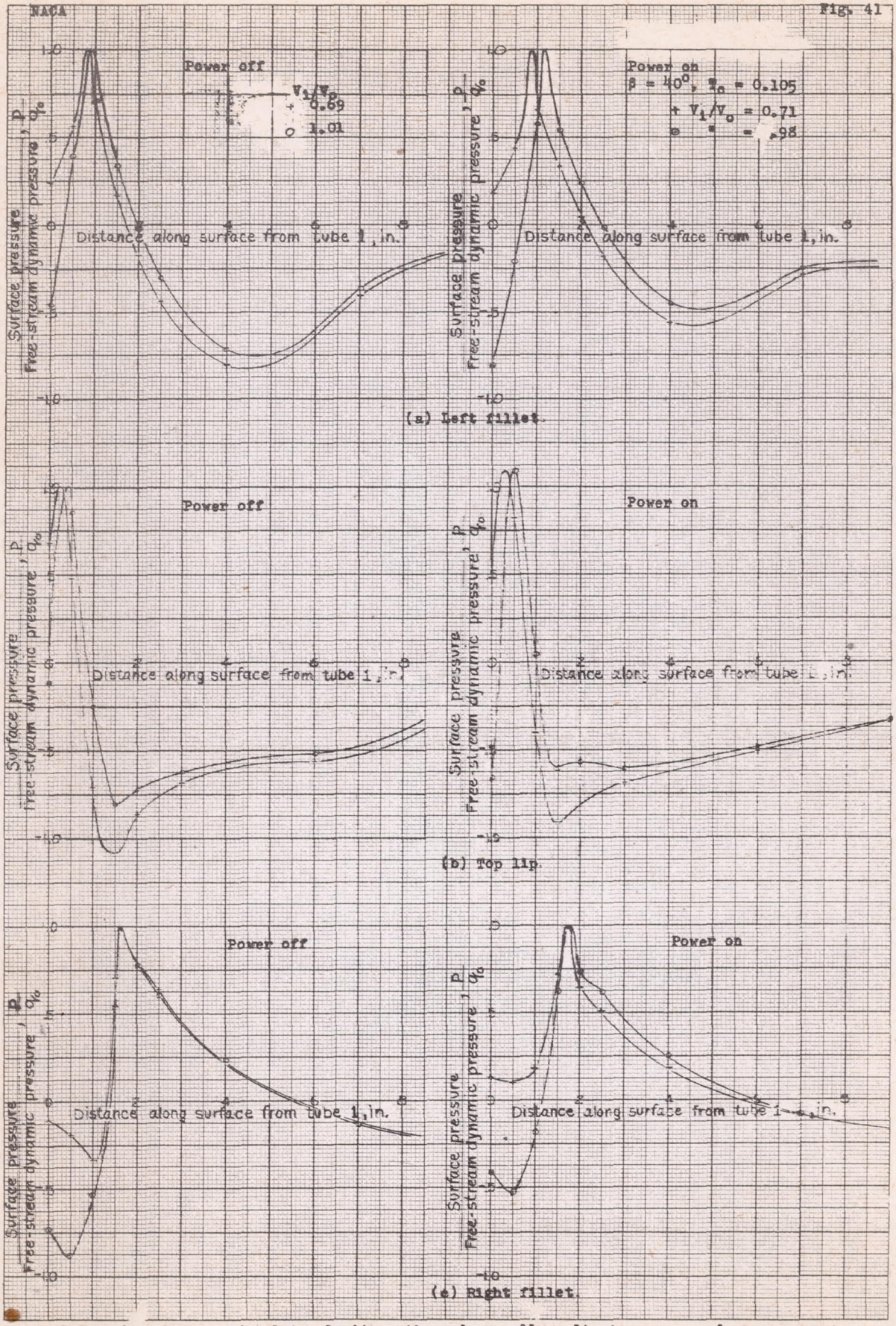

Figure 41.- Effect of inlet-velocity ratio and propeller slipstream on surface pressure; scoop 5, $\alpha = 6^o$, climb condition; Mach number 0.08.